Fluorinated Distyrylbenzene Chromophores: Effect of Fluorine Regiochemistry on Molecular Properties and Solid-State Organization

Michelle L. Renak,[†] Glenn P. Bartholomew,[‡] Shujun Wang,[‡] Pascal J. Ricatto,[†,§] Rene J. Lachicotte,[†] and Guillermo C. Bazan*[,‡]

Contribution from the Department of Chemistry, University of Rochester, Rochester, New York, 14627-0216, Department of Chemistry, University of California, Santa Barbara, California 93106, and Bergen Community College, Paramus, New Jersey 07652

Received December 28, 1998. Revised Manuscript Received June 7, 1999

Abstract: A series of fluorinated distyrylbenzene (**DSB**) derivatives were synthesized and studied in order to probe the effect of fluorine substitution on molecular properties and on the arrangement of molecules in the solid state. Reaction of 1,4-diiodobenzene with 4-fluorostyrene or pentafluorostyrene in the presence of $Pd(OAc)_2$ gives *trans-trans*-bis(4-fluorostyryl)benzene (**2F$_t$**) and *trans-trans*-1,4-bis(pentafluorostyryl)benzene (**10F$_t$**), respectively. Bis(2,5-difluorostyryl)benzene (**4F$_t$**) was prepared by the reaction of 2,5-difluorobenzaldehyde with *p*-xylylenebis-(triphenylphosphonium bromide) in the presence of LiOEt in EtOH. Coupling of 1,4-dibromo-2,5-difluorobenzene with styrene, 4-fluorostyrene, or pentafluorostyrene using $Pd(OAc)_2$ gives 1,4-bis(styryl)-2,5-difluorobenzene (**2F$_c$**), 1,4-bis(4-fluorostyryl)-2,5-difluorobenzene (**2F$_c$2F$_t$**), and 1,4-bis-(pentafluorostyryl)-2,5-difluorobenzene (**2F$_c$10F$_t$**), respectively. Absorption spectroscopy shows that **DSB**, **2F$_t$**, **2F$_c$**, **2F$_c$2F$_t$**, **4F$_t$**, **10F$_t$**, and **2F$_c$10F$_t$** have a λ_{max} at approximately 350 nm. Addition of dimethylaniline to hexane solutions results in exciplex emission with λ_{max} ranging from 458 to 514 nm, depending on fluorine regiochemistry. Cyclic voltammetry shows that, as the fluorine load increases, the reduction of the **DSB** framework becomes more facile. It is also shown that the regiochemistry of substitution makes an impact on the inductive ability of fluorine to facilitate reduction. The lattice properties of **2F$_c$**, **2F$_c$2F$_t$**, **4F$_t$**, **10F$_t$**, and **2F$_c$10F$_t$** were determined by X-ray diffraction experiments. Two structural motifs emerge from these studies. One is the tendency of the **DSB** framework to stack cofacially and form vertical "columns" within the crystal. The second motif is the alignment of these "columns" to maximize C−H···F electrostatic registry.

Introduction

There is widespread interest in the use of conjugated organic materials in emerging optoelectronic technologies.[1] Part of the interest stems from the control and flexibility that organic methodology affords over chemical groups on a given carbon framework. By careful choice of functionality it is possible to fine-tune important electronic properties.[2] Electron-donating or -withdrawing substituents may raise or lower the energies of the highest occupied molecular orbital (HOMO) and the lowest unoccupied molecular orbital (LUMO) differently, allowing for modulation of the molecular "band gap".[3] Sufficient types of conjugated polymers and small molecules have appeared that emission from organic-based light-emitting diodes (LEDs) covers the entire visible spectrum.[4] Pendant groups with varying degrees of steric properties may be used to optimize emission quantum yield and solubility.[5] For example, poly [2-(2′-ethylhexyloxy)-5-methoxy-1,4-phenylenevinylene) (MEH−PPV) is a soluble conjugated polymer that can be cast from solution and used as the electroluminescent layer in LEDs.[6]

Attaching electron-withdrawing[7] or -donating[8] groups on a carbon framework changes the redox properties and optical performance of the molecule.[9] These properties ultimately affect the charge transport characteristics of the bulk and define the role that the material may play in different device configurations. Organic molecules are generally better hole transport materials than electron transport materials, and significant efforts are

[†] University of Rochester.
[‡] University of California, Santa Barbara.
[§] Bergen Community College.

(1) (a) Sheats, J. R.; Antoniadis, H.; Hueschen, M.; Leaonard, W.; Miller, J.; Moon, R.; Roitman, D.; Stocking, A. *Science* **1996**, *273*, 884. (b) Gymer, R. W. *Endeavour* **1996**, *20* (3), 115. (c) Friend, R. H.; Denton, G. J.; Halls, J. J. M.; Harrison, N. T.; Holmes, A. B.; Köhler, A.; Lux, A.; Moratti, S. C.; Pichler, K.; Tessler, N.; Towns, K. *Synth. Met.* **1997**, *84*, 463. (d) Hide, F.; Díaz-García, M. A.; Schwartz, B. J.; Heeger, A. J. *Acc. Chem. Res.* **1997**, *30*, 430. (e) Maniloff, E.; Vacar, D.; McBranch, D.; Wang, H.-L.; Mattes, B.; Heeger, A. J. *Synth. Met.* **1997**, *84*, 547. (f) Bao, Z.; Lovinger, A. J.; Brown, J. *J. Am. Chem. Soc.* **1998**, *120*, 207. (g) Roth, S. *Synth. Met.* **1993**, *55*−*57*, 3623.

(2) (a) Burn, P. L.; Kraft, A.; Baigent, D. R.; Bradley, D. D. C.; Brown, A. R.; Friend, R. H.; Gymer, R. W.; Holmes, A. B.; Jackson, R. W. *J. Am. Chem. Soc.* **1993**, *115*, 10117. (b) Adachi, C.; Nagai, K.; Tamoto, N. *Appl. Phys. Lett.* **1995**, *66* (20), 2679.

(3) (a) Moratti, S. C.; Cervini, R.; Holmes, A. B.; Baigent, D. R.; Friend, R. H.; Greenham, N. C.; Grüner, J.; Hamer, P. J. *Synth. Met.* **1995**, *71*, 2117. (b) Höger, S.; McNamara, J. J.; Schricker, S.; Wudl, F. *Chem. Mater.* **1994**, *6*, 171.

(4) (a) Tang C. W.; VanSlyke, A. *Appl. Phys. Lett.* **1987**, *51* (12), 913. (b) Burroughes, J. H.; Bradley, D. D. C.; Brown, A. R.; Marks, R. N.; Mackay, K.; Friend, R. H.; Burns, P. L.; Holmes, A. B. *Nature* **1990**, *347*, 539. (c) Kido, J.; Hayase, H.; Hongawa, K.; Nagai, K.; Okuyama, K. *Appl. Phys. Lett.* **1994**, *65* (17), 2124. (d) Kido, J.; Kimura, M.; Katsutoshi, N. *Science* **1995**, *267*, 1332. (e) Huang, W.; Meng, H.; Yu, W.-L.; Gao, J.; Heeger, A. J. *Adv. Mater.* **1998**, *10* (8), 593.

(5) Kraft, A.; Grimsdale, A. C.; Holmes, A. B. *Angew. Chem., Int. Ed.* **1998**, *37*, 402.

(6) Braun, D.; Heeger, A. J. *Appl. Phys. Lett.* **1991**, *58* (18), 1982.

(7) Lux, A.; Holmes, A. B.; Cervini, R.; Davies, J. E.; Moratti, S. C.; Grüner, J.; Cacialli, F.; Friend, R. H. *Synth. Met.* **1997**, *84*, 293.

(8) Ndayikengurukiye, H.; Jacobs, S.; Tachelet, W.; Van Der Looy, J.; Pollaris, A.; Geise, H. J.; Claeys, M.; Kauffmann, J. M.; Janietz, S. *Tetrahedron* **1997**, *53* (40), 13811.

(9) Brédas, J. *Adv. Mater.* **1995**, *7* (3), 263.

10.1021/ja984440q CCC: $18.00
Published on Web 08/13/1999

focused on designing durable electron transport materials with high mobilities.[10] Attaching electronegative functionalities, such as cyano groups, onto emissive polymers such as poly(*p*-phenylenevinylene) (PPV) facilitates electron injection.[11] Fluorinated PPV has also been successfully synthesized[12] and found to have a lower band gap than PPV.[13]

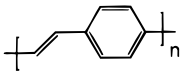

PPV

Recent experimental work has also demonstrated that the ability of organic materials in a given device configuration is also strongly influenced by the morphology of the bulk. Charge transport in organic field-effect transistors depends on the electronic overlap between molecules and thus their relative orientation.[14] Overall performance is determined by crystal size and by the spatial placement of molecules.[15] For LEDs, the film forming properties of organic materials affect their efficiency and reliability. Amorphous thin films give excellent device performance.[16] Ordered regions within emissive layers of polymer LEDs act as exciton traps and thus reduce the internal efficiency of the device.[17] In response to these complications there is considerable interest in the design of disordered solids.[18,19] Bulky substitutents and dendritic structures discourage polymer chains from packing tightly and forming crystalline domains.[20] The arrangement of small molecules in the solid state can also be adjusted using a tetrahedral junction.[21]

Chemical groups and molecular topology therefore control the performance of a material by modifying the electronic and optical properties of individual molecules and by influencing their solid-state arrangement. It is difficult, even for a closely related family of compounds, to predict molecular association and foresee how a given morphology will influence the optical properties of the condensed state. For polymeric compounds, these problems are further accentuated by the coexistence of crystalline and amorphous regions and by the statistical nature of most polymerization reactions which gives a distribution of chain lengths.[22] To circumvent these problems, well-defined molecular models, that is, oligomers that are representative of important polymer families, have been successfully used to examine structure−property relationships.[23,24]

In this contribution, we report on a versatile synthesis of fluorinated organic chromophores via Heck and Wittig reactions. Specifically, the focus is on the distyrylbenzene (**DSB**) framework which has been studied previously because of its structural relationship to PPV and other emissive polymers.[25]

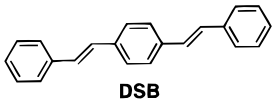

DSB

The impact of fluorine regiochemistry on the optical and electronic properties of solvated molecules is measured by solution spectroscopic and electrochemical techniques and by exciplex formation with dimethylaniline. In addition, we examine the impact of fluorine substitution on morphology by X-ray crystallography and by looking at phase transitions using calorimetry. The aim of this study is to probe how fluorine substitution affects molecular and solid-state properties. The long-range goal is to understand the relationship between molecular connectivity and the collective optical behavior of organic solids.

Results

Synthesis. There is no convenient method for chemically exchanging the hydrogen atoms in **DSB** for fluorine. The Heck reaction, using appropriately substituted commercially available styrenes with 1,4-dihalobenzenes, allows one to build the **DSB** framework in a modular fashion. For example, the reaction of 1,4-diiodobenzene with two equivalents of 4-fluorostyrene produces *trans*,*trans*-bis(4-fluorostyryl)benzene (**2F$_t$** in eq 1).

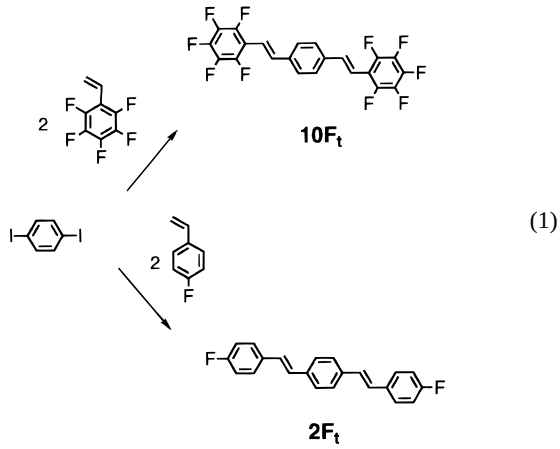

10F$_t$

2F$_t$

(1)

The best results are obtained when the reaction is carried out in *N*,*N*-dimethylacetamide using $Pd(OAc)_2$ under phase-transfer conditions (nBu$_4$NBr and K_2CO_3) over a period of 36 h.[26] Standard work up provides **2F$_t$** as a pale yellow powder in 50% yield. The all-trans conformation is obtained from the Heck protocols, as determined by the J_{HH} values of the olefinic

(10) Strukelj, M.; Papadimitrakopoulos, F.; Miller, T. M.; Rothberg, L. J. *Science* **1995**, *267*, 1969.
(11) Greenham, N. C.; Moratti, S. C.; Bradley, D. D. C.; Friend, R. H.; Holmes, A. B. *Nature* **1993**, *365*, 628.
(12) (a) Benjamin, I.; Faraggi, E. Z.; Avny, Y.; Davidov, D.; Neumann, R. *Chem. Mater.* **1996**, *8*, 352. (b) Kang, I.-N.; Shim, H.-K.; Zyung, T. *Chem. Mater.* **1997**, *9*, 746.
(13) Gurge, R. M.; Sarker, A. M.; Lahti, P. M.; Hu, B.; Karasz, F. E. *Macromolecules* **1997**, *30*, 8286.
(14) Li, X.-C.; Sirringhaus, H.; Garnier, F.; Holmes, A. B.; Moratti, S. C.; Feeder, N.; Clegg, W.; Teat, S. J.; Friend, R. H. *J. Am. Chem. Soc.* **1998**, *120*, 2206.
(15) Laquindanum, J. G.; Katz, H. E.; Lovinger, A. J. *J. Am. Chem. Soc.* **1998**, *120*, 664.
(16) Adachi, C.; Tsutsui, T.; Saito, S. *Appl. Phys. Lett.* **1990**, *56* (9), 799.
(17) Conwell, E. *Trends Polym.* Sci. **1997**, *5*, 218.
(18) (a) Thelakkat, M.; Fink, R.; Huabner, F.; Schmidt, H.-W. *Macromol. Symp.* **1997**, *125*, 157. (b) Thelakkat, M.; Schmidt, H.-W. *Adv. Mater.* **1998**, *10* (3), 219.
(19) Son, S.; Dodabalapur, A.; Lovinger, A. J.; Galvin, M. E. *Science* **1995**, *269*, 376.
(20) Chung, S.-J.; Jin, J.-I.; Lee, C.-H.; Lee, C.-E. *Adv. Mater.* **1998**, *10* (9), 684. (b) Deb, S. K.; Maddux, T. M.; Yu, L. *J. Am. Chem. Soc.* **1997**, *119*, 9079.
(21) Oldham, W. J.; Lachicotte, R. J.; Bazan, G. C. *J. Am. Chem. Soc.* **1998**, *120*, 2987.
(22) Miao, Y.-J.; Herkstroeter, W. G.; Sun, B. J.; W.-F., A. G.; Bazan, G. C. *J. Am. Chem. Soc.* **1995**, *117*, 11407.
(23) (a) Müllen, K.; Wegner, G. *Adv. Mater.* **1998**, *10* (6), 433. (b) Schenk, R.; Gregorius, H.; Meerholz, K.; Heinze, J.; Müllen, K. *J. Am. Chem. Soc.* **1991**, *113*, 2634. (c) Dottinger, S. E.; Hohloch, M.; Segura, J. L.; Steinhuber, E.; Hanack, M.; Tompert, A.; Oelkrug, D. *Adv. Mater.* **1997**, *9* (3), 233.
(24) Strehmel, B.; Sarker, A. M.; Malpert, J. H.; Strehmel, V.; Seifert, H.; Neckers, D. C. *J. Am. Chem. Soc.* **1999**, *121*, 1226.
(25) (a) Colaneri, N. F.; Bradley, D. D. C.; Friend, R. H.; Burn, P. L.; Holmes, A. B.; Spangler, C. W. *Phys. Rev. B* **1990**, *42* (18), 11, 670. (b) Dottinger, S. E.; Hohloch, M.; Hohnholz, D.; Segura, J. L.; Steinhuber, E.; Hanack, M. *Synth. Met.* **1997**, *84*, 267.
(26) Jeffery, T. In *Advances in Metal-Organic Chemistry*; Liebeskind, L. S., Eds; JAI Press Inc.: Connecticut, 1996; Vol. 5, pp 188−191.

resonances in the ^{1}H NMR spectra. The reaction of 2 equiv of pentafluorostyrene and 1,4-diiodobenzene proceeds similarly to give *trans-trans*-1,4-bis(pentafluorostyryl)benzene (**10F$_t$** in eq 1) in 63% yield. Compound **10F$_t$** is considerably more soluble than **2F$_t$** in standard organic solvents. For example, the solubility of **10F$_t$** is 6.2 mg/mL in THF at room temperature whereas the solubility of **2F$_t$** is only 1.8 mg/mL.

Bis(2,5-difluorostyryl)benzene (**4F$_t$** in eq 2) is obtained by

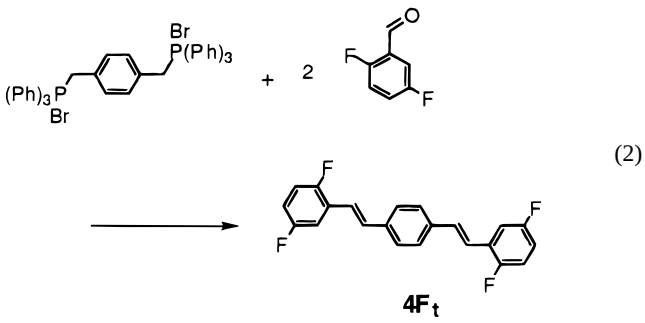

(2)

coupling two equivalents of 2,5-difluorobenzaldehyde with *p*-xylylenebis(triphenylphosphonium bromide) in the presence of LiOEt in EtOH. The reaction proceeds in relatively low yield and gives a mixture of trans−trans, cis−trans, and cis−cis isomers. The mixture of isomers can be converted to the trans−trans isomer by refluxing a xylene solution in the presence of a catalytic amount of iodine.

1,4-Dibromo-2,5-difluorobenzene provides the module for building **DSB** derivatives containing a doubly fluorinated central ring. Thus, reaction with styrene, 4-fluorostyrene, or pentafluorostyrene, under Heck conditions, affords 1,4-bis(styryl)-2,5-difluorobenzene (**2F$_c$**), 1,4-bis(4-fluorostyryl)-2,5-difluorobenzene (**2F$_c$2F$_t$**), and 1,4-bis(pentafluorostyryl)-2,5-difluorobenzene (**2F$_c$10F$_t$**), respectively (eq 3).

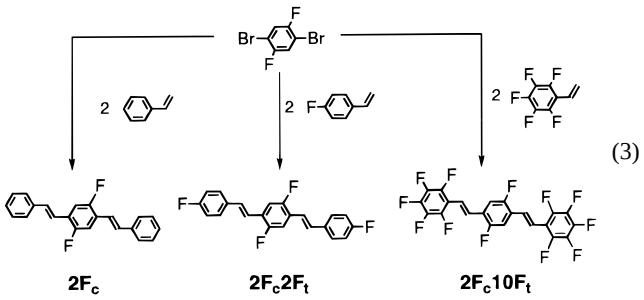

(3)

Analysis by ^{1}H NMR spectroscopy provides a convenient method for confirming fluorine regiochemistry and alkene stereochemistry. All spectra were assigned by a combination of heteronuclear and homonuclear decoupling techniques. In many instances second-order spectra were observed (Figure 1).

Optical Spectroscopy. Absorption and fluorescence emission spectra were measured to monitor the effect of fluorine substitution on the HOMO−LUMO energy gap. Comparison of the spectra shows minimal changes upon fluorine substitution (Table 1). The largest difference is between **2F$_c$** and **10F$_t$**, which differ in their absorption maxima by 9 nm and their emission maxima by 14 nm (Figure 2). Altogether, these data show that color variation by fluorine substitution is minimal, and consequently, the HOMO−LUMO gap (∼3.5 eV) can be considered essentially constant for the entire series of compounds.

Photoluminescence quantum yields (Φ_{PL}) were determined in cyclohexane using 9,10-diphenylanthracene as the standard.[27]

(27) Hamai, S.; Hirayama, F. *J. Phys. Chem.* **1983**, *87*, 83.

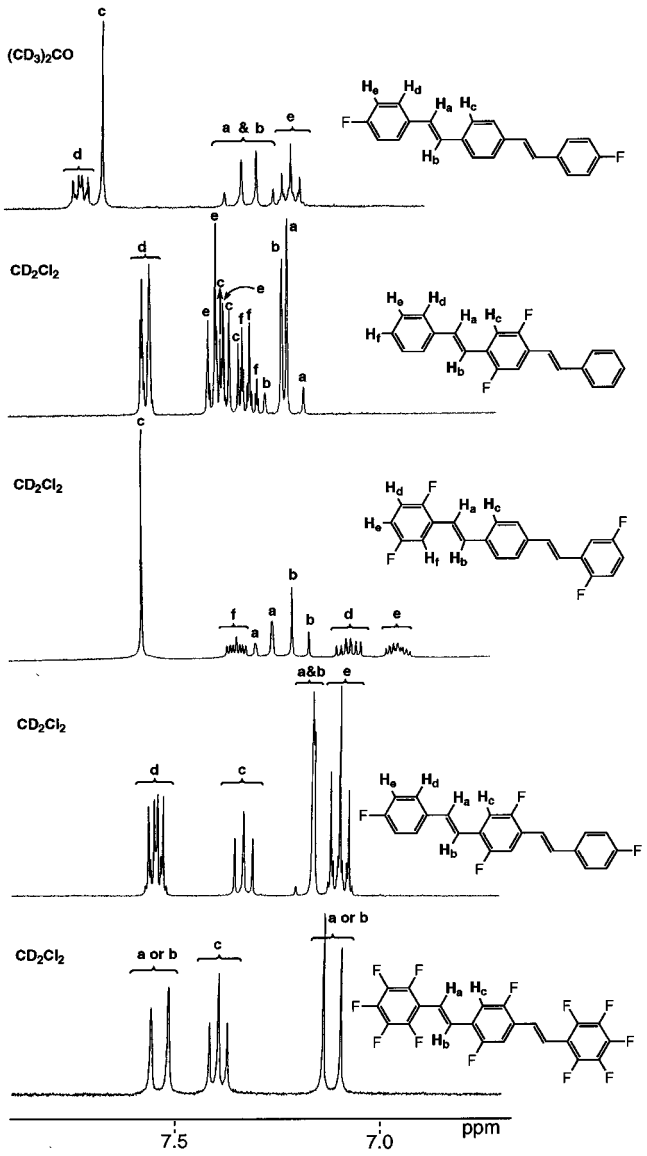

Figure 1. ^{1}H NMR spectra of **2F$_t$**, **2F$_c$**, **4F$_t$**, **2F$_c$2F$_t$**, and **2F$_c$10F$_t$**.

Table 1. Absorption and Fluorescence Data and Photoluminescence (PL) Quantum Yields in Cyclohexane

compound	absorbance maximum (nm)	emission maximum (nm)	PL quantum efficiency
DSB	350	405	0.77
2F$_c$	357	415	0.70
2F$_t$	350	403	0.76
2F$_c$2F$_t$	358	415	0.67
4F$_t$	355	410	0.68
10F$_t$	348	401	0.078
2F$_c$10F$_t$	351	409	0.68

The calculated Φ_{PL} values are centered near 70% for the majority of the molecules (Table 1). The notable exception is **10F$_t$**, for which Φ_{PL} is on the order of 8%. Fluorescence lifetime measurements were performed to probe the excited-state dynamics, and the resulting decay profiles for **DSB**, **10F$_t$**, and **2F$_c$10F$_t$** are shown in Figure 3. The fluorescence intensities of **DSB** and **2F$_c$10F$_t$** decay monoexponentially ($\tau = 1.52$ ns) and are indistinguishable. In contrast, the decay for **10F$_t$** can be expressed as a biexponetial function with $\tau_1 = 300$ ps (94%) and $\tau_2 = 600$ ps (6%).

Possible nonradiative decay pathways for **10F$_t$** include excimer formation (i.e., self-quenching) and intramolecular

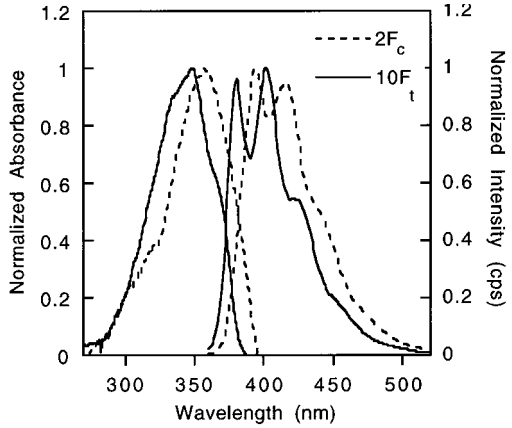

Figure 2. Absorption and fluorescence emission spectra (excitation $\lambda = 350$ nm) of $\mathbf{2F_c}$ and $\mathbf{10F_t}$ in cyclohexane.

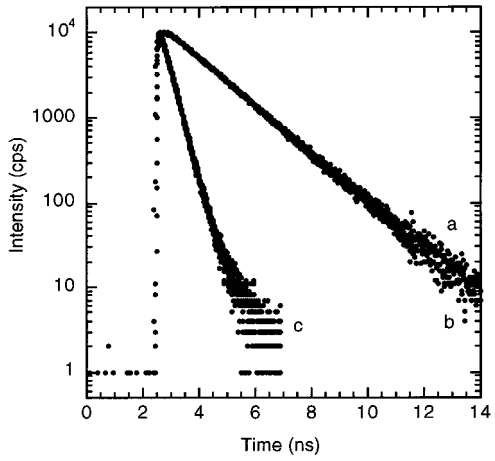

Figure 3. Time-resolved fluorescence emission spectra of (a) **DSB**, (b) $\mathbf{2F_c10F_t}$, and (c) $\mathbf{10F_t}$ in cyclohexane (excitation $\lambda = 355$ nm; observed emission $\lambda = 400$ nm).

vibrational or rotational motions.[28] Since the steady-state fluorescence emission spectra were measured for both $\mathbf{10F_t}$ and $\mathbf{2F_c10F_t}$ in dilute solution (8.33×10^{-7} M), the bimolecular pathway can be ruled out. Changing the solvent from hexane to more viscous hexadecane[29] causes the Φ_{PL} of $\mathbf{10F_t}$ to increase from 8% to 15%. These results suggest that the low Φ_{PL} values of $\mathbf{10F_t}$ are probably a result of excited-state deactivation by rotation about the double bonds.[30] That irradiation of the trans−trans isomer of $\mathbf{10F_t}$ at 375 nm forms the trans−cis isomer provides additional evidence for photoinduced olefin isomerization.[31]

Tuning Emission Frequency via Exciplex Formation. Optical spectroscopy measurements show that fluorine substitution on **DSB** does not affect the HOMO−LUMO energy difference. One way to tune the emission color for this series of compounds is through exciplex formation. This strategy has been used to tune the emission color of conjugated polymers and small molecules.[32] Efficient blue luminescence has been realized from polybenzobisthiazoles and tris(*p*-tolyl)amine.[33] Orange and red electroluminescence has also been observed from exciplexes that form at the interface between layers of *N*,*N*′-diphenyl-*N*,*N*′-bis(3-methylphenyl)-[1,1′-biphenyl]-4,4′-diamine (TPD) and quinoxaline derivatives.[34] The ill defined nature of these mixtures makes it difficult to correlate chromophore properties with frequency of emission. Because the structure of the fluorinated DSBs are well defined, we thought that they would be ideal study candidates for probing exciplex formation with a suitable donor.

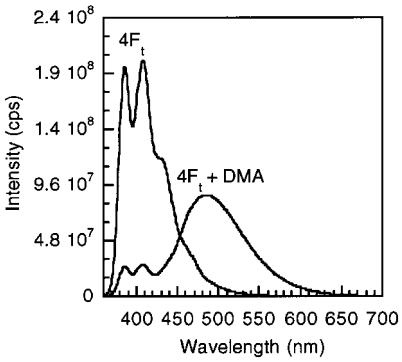

Figure 4. Fluorescence emission spectra ($\lambda_{excitation} = 350$ nm) of $\mathbf{4F_t}$ (3×10^{-6} M) and of $\mathbf{4F_t}$ (3×10^{-6} M) and *N*,*N*-dimethylaniline (0.1 M) in hexanes.

Exciplex formation was investigated using *N*,*N*-dimethylaniline (DMA). Figure 4 shows the emission spectra of $\mathbf{4F_t}$ and $\mathbf{4F_t}$ with DMA in hexanes. These data are representative of the fluorescent properties for all of the DSB/DMA pairs. In the presence of DMA, the emission for $\mathbf{4F_t}$ in hexanes diminishes with concomitant appearance of exciplex emission, ($\mathbf{4F_t}$/DMA)*, at longer wavelengths. Exciplex emission decreases in intensity and shifts to lower energy upon changing the solvent from hexanes to toluene. In tetrahydrofuran, exciplex emission is not observed, presumably because the more polar medium favors formation of solvent separated ion pairs.[35] The absorption spectrum of a solution of $\mathbf{4F_t}$ with DMA is a composite of the spectra of the individual solutions. Thus, we rule out direct excitation of a ground-state complex.

The frequency of exciplex emission depends on fluorine substitution. The corrected fluorescence spectra for all of the fluorinated DSB/DMA pairs, normalized to equal intensity, are shown in Figure 5. Overall, the exciplex emission shifts to lower energy with increasing numbers of fluorine atoms (Table 2). Closer inspection reveals that, while the emission wavelength maximum for ($\mathbf{2F_t}$/DMA)* is nearly identical to that for (**DSB**/DMA)*, the band for ($\mathbf{2F_c}$/DMA)* occurs at longer wavelengths. Additionally, the emission maximum for ($\mathbf{2F_c2F_t}$/DMA)* is coincident with that of ($\mathbf{2F_c}$/DMA)*. These data indicate that the fluorines on the terminal rings of $\mathbf{2F_t}$ and $\mathbf{2F_c2F_t}$ do not influence significantly the energy of the exciplex emission (Table 2).

The total photoluminescence quantum yields (Φ_{Total}), which include residual monomer emission together with exciplex

(28) Turro, N. J.; *Modern Molecular Photochemistry*; University Science Books: Sausalito, CA, 1991.

(29) The viscosity of hexanes and hexadecane at 20 °C is 0.326 and 3.34 cp, respectively (cp = centipoises). Weast, R. C., Astle, M. J., Beyer, W. H., Eds. *Handbook of Chemistry and Physics*, 68th ed.; CRC Press: Boca Raton, FL, 1987; p F42.

(30) (a) Saltiel, J.; Zafiriou, O. C.; Magarity, E. D.; Lamola E. D. *J. Am. Chem. Soc.* **1968**, *90*, 4759. (b) Sharafy, S.; Muszkat, K. A. *J. Am. Chem. Soc.* **1971**, *93*, 4119.

(31) The conversion from the trans−trans to the trans−cis isomer of $\mathbf{10F_t}$ is shown by ^{1}H NMR spectroscopy. For the cis−trans isomer: ^{1}H NMR (C_6D_6) δ 7.17 (d, 1H, vinylene), 7.02 (d, 2H, $J_{HH} = 8.4$ Hz), 6.90 (d, 2H, $J_{HH} = 8.4$ Hz), 6.68 (d, 1H, vinylene, $J_{HH} = 16.4$ Hz), 6.54 (d, 1H, vinylene, $J_{HH} = 12$ Hz), 5.84 (d, 1H, vinylene, $J_{HH} = 13$ Hz).

(32) Weller, A. *The Exciplex*; Gordon, M., Ware, W. R., Eds.; Academic Press Inc.: New York, 1975.

(33) Jenekhe, S. A.; Osaheni, J. A. *Science* **1994**, *265*, 765.

(34) Wang, J.-F.; Kawabe, Y.; Shaheen, S. E.; Morrell, M. M.; Jabbour, G. E.; Lee, P. A.; Anderson, J.; Armstrong, N. R.; Kippelen, B.; Mash, E. A.; Peyghambarian, N. *Adv. Mater.* **1998**, *10* (3), 230.

(35) (a) Rhem, D.; Weller, A. *Isr. J. Chem.* **1970**, *8*, 259. (b) Rhem, D.; Weller, A. *Z. Phys. Chem.* **1970**, *69*, 183.

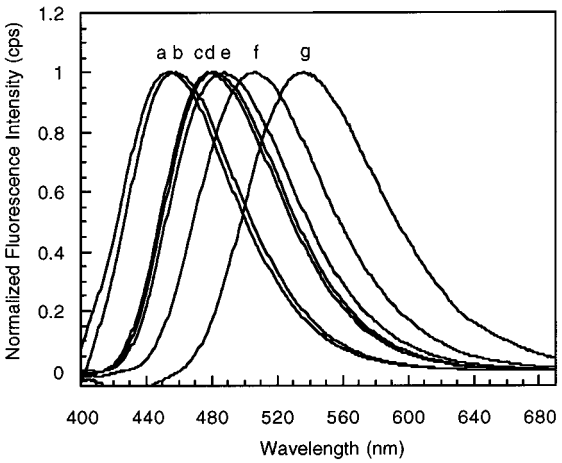

Figure 5. Fluorescence emission spectra ($\lambda_{excitation}$ = 350 nm) of solutions of dimethylaniline (0.1 M) and (a) **2F$_t$**, (b) **DSB**, (c) **2F$_c$2F$_t$**, (d) **2F$_c$**, (e) **4F$_t$**, (f) **10F$_t$**, and (g) **2F$_c$10F$_t$** (All DSBs = 3×10^{-6} M) in hexanes. The exciplex band is obtained by subtracting the normalized total emission spectra from the emission spectra of monomer.

Table 2. Exciplex Data for Distyrylbenzene Derivatives with DMA (0.1M) in Hexanes[a]

compound	exciplex emission λ_{max} (nm)	Φ_{Total}[b]	$\Phi_{residual}$[c]	Φ_{ex}[d]
DSB	458	0.72	0.19 (26%)	0.53 (74%)
2F$_t$	454	0.66	0.18 (27%)	0.49 (73%)
2F$_c$	482	0.42	0.091 (22%)	0.32 (78%)
2F$_c$2F$_t$	481	0.42	0.088 (21%)	0.33 (79%)
4F$_t$	488	0.53	0.088 (17%)	0.44 (83%)
10F$_t$	506	0.34	0.049 (15%)	0.29 (85%)
2F$_c$10F$_t$	514	0.13	0.083 (66%)	0.043 (34%)

[a] Experimental uncertainties of the values are estimated to ~5%. [b] Total quantum yields of residual monomer emission and exciplex emission obtained in hexanes in the presence of 0.1 M DMA. [c] Quantum yields of residual monomer emission in hexanes in the presence of 0.1 M DMA; values in parentheses are the contributions to total emission. [d] Quantum yields of exciplex emission in hexanes in the presence of 0.1 M DMA; values in parentheses are the contributions of exciplex emission to total emission.

emission (at 0.1 M DMA), were determined in hexanes. These yields were determined from comparisons against solutions of the corresponding monomer (Table 1). The Φ_{Total} was further broken down into residual monomer ($\Phi_{residual}$) and exciplex emission (Φ_{ex}) (Table 2). Comparison of the entries in Table 2 shows that the overall emission is quenched by the addition of DMA. The drop in emission ranges from 6% for **DSB** to 81% for **2F$_c$10F$_t$**. One exception occurs with **10F$_t$**, for which the overall emission in the presence of DMA shows a 4.4-fold enhancement. Exciplex emission under these conditions dominates the total emission, except for **2F$_c$10F$_t$**, for which only 34% of Φ_{Total} is from exciplex emission. Generally, Φ_{ex} decreases with the increasing number of fluorination, with Φ_{ex} = 0.53, 0.49, 0.44, 0.29, and 0.043 for **DSB**, **2F$_t$**, **4F$_t$**, **10F$_t$**, and **2F$_c$10F$_t$**, respectively. As is the case for the emission frequency, fluorine substitution on the terminal rings does not affect the magnitude of Φ_{Total} or the breakdown of Φ_{Total} into exciplex and monomer components. Overall, the results show that, although the emission frequencies of the DSB derivatives are nearly constant, it is possible to tune the emission wavelength in hexanes from 458 to 514 nm by the addition of DMA.

Electrochemistry. Absorption spectroscopy allows for an estimate of HOMO−LUMO energy differences. To establish absolute energies, we measured the reduction potential of all of the compounds by cyclic voltammetry (CV). The results of this study are collected in Table 3. Precautions were taken to ensure a rigorously oxygen- and moisture-free (nBu$_4$N)(PF$_6$)/THF electrolyte/solvent medium.[36] Decamethyferrocene (Me$_{10}$-Fc) was used as the internal standard and was referenced to ferrocene (Fc, 0.449 V versus Me$_{10}$Fc in THF).[37] The reduction potentials in Table 3 are reported versus the Fc/Fc$^+$ couple. Repeated measurements showed that the reduction potential for a given compound, under identical experimental conditions, is reproducible to ±0.01 V.

Table 3. Reduction Potentials of **DSB**, **2F$_c$**, **2F$_t$**, **2F$_c$2F$_t$**, **4F$_t$**, **10F$_t$**, and **2F$_c$10F$_t$**[a]

compound	$E°_1$(V)[b]	$E°_2$(V)[b]	compound	$E°_1$(V)[b]	$E°_2$(V)[b]
DSB	−2.48	−2.74	**4F$_t$**	−2.25	−2.44
2F$_t$	−2.47	−2.79	**10F$_t$**[c]	−2.09	−2.25
2F$_c$	−2.25	−2.59	**2F$_c$10F$_t$**	−1.91	−2.10
2F$_c$2F$_t$	−2.23	−2.58			

[a] Conditions: C = 0.001 M analyte in 0.2 M (nBu$_4$N)(PF$_6$)/THF electrolyte, scan rate = 200 mV/s, RT, Pt disk working electrode, Pt wire counter electrode, and bare silver reference electrode. [b] Potentials reported versus ferrocene/ferrocenium couple. [c] Measured at −8 °C.

The entries in Table 3 indicate that, in general, the electron affinity increases with an increasing number of fluorine atoms. A trend of this type is expected on the basis of increased charge induction around the periphery of the distyrylbenzene framework. More significant is the observation that the location of fluorine substitution influences the reduction potential and the stability of the reduced species formed under our experimental conditions. Figure 6 contains the cyclic voltammograms of **2F$_c$** and **10F$_t$**. The more highly fluorinated compounds, **10F$_t$** and **2F$_c$10F$_t$**, show irreversible reductions whereas the other compounds show reversible reduction waves.

DSB shows a one electron reversible wave corresponding to the **DSB**/**DSB**$^-$ couple at −2.48 V, followed by a second reduction at −2.74 V.[38] The fluorines at the 2 and 5 positions of the inner ring of **2F$_c$** change the first reduction potential of the **DSB** framework to −2.25 V (Table 3), indicating a more accessible radical anion. The reduction potentials of **2F$_t$** (Table 3) are nearly identical to those of **DSB**. Fluorine atoms at the 4′ and 4″ positions (see numbering scheme below) therefore do not greatly perturb the electron affinity of the carbon framework. The overall electrochemical behavior of **2F$_t$**, however, differs from that of **DSB**. The value of i_{ap}/i_{cp} (anodic peak current/cathodic peak current)[39] for the first cathodic wave of **2F$_t$** is less than 1.0 at scan rates below 3200 mV/s. Therefore, relative to **DSB** the first reduction of **2F$_t$** is quasi-reversible, indicating the formation of a less stable radical anion.

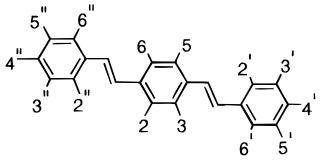

The redox properties of **2F$_c$2F$_t$** are nearly identical to those of **2F$_c$** (Table 3). The terminal fluorine atoms do not significantly change the reduction potentials of **2F$_c$2F$_t$** from that of **2F$_c$** or affect the stability of the radical anion formed. For **4F$_t$** a reversible one electron cathodic wave at −2.25 V is followed

(36) Meerholz, K.; Heinze, J. *J. Am. Chem. Soc.* **1989**, *111*, 2325.
(37) We thank Prof. William Geiger for providing these measurements.
(38) Heinze, J.; Mortensen, J.; Müllen, K.; Schenk, R. *J. Chem. Soc., Chem. Commun.* **1987**, 701.
(39) Nicholson, R. S. *Anal. Chem.* **1966**, *38*, 1406.

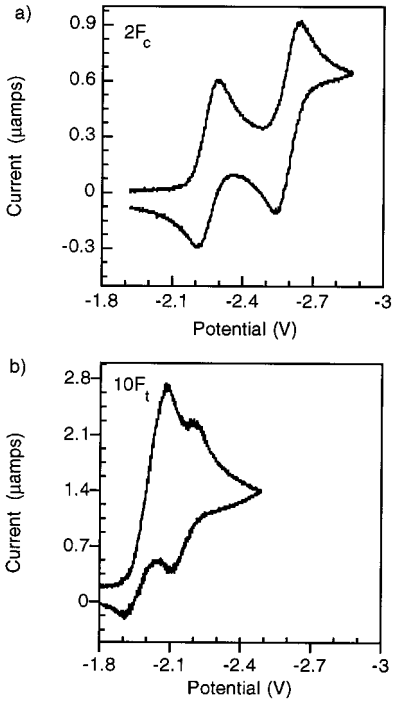

Figure 6. Cyclic voltammograms illustrating the reduction of (a) $\mathbf{2F_c}$ and (b) $\mathbf{10F_t}$. Measurements were performed with the analyte (0.001 M) in 0.2 M (nBu$_4$N)(PF$_6$)/THF at a scan rate of 200 mV/s at room temperature for $\mathbf{2F_c}$ and at −8 °C for $\mathbf{10F_t}$. Potentials are referenced to ferrocene.

Table 4. LUMO and HOMO Energy Levels

compound	LUMO energy (eV)[a]	λ_{onset} (nm)	HOMO−LUMO gap (eV)[b]	calculated HOMO energy (eV)
DSB	−2.79	387	3.20	−5.99
$\mathbf{2F_t}$	−2.80	385	3.22	−6.02
$\mathbf{2F_c}$	−3.02	394	3.15	−6.17
$\mathbf{2F_c2F_t}$	−3.04	394	3.15	−6.19
$\mathbf{4F_t}$	−3.02	390	3.18	−6.20
$\mathbf{10F_t}$	−3.18	382	3.25	−6.43
$\mathbf{2F_c10F_t}$	−3.36	388	3.19	−6.55

[a] From cyclic voltammetry data. [b] From absorption spectra.

by a second reduction at −2.58 V. The potentials for the first reduction of $\mathbf{2F_c}$ and $\mathbf{4F_t}$ are thus identical. The second reduction for $\mathbf{4F_t}$ occurs at less negative potentials than for $\mathbf{2F_c}$. It seems that the fluorine atoms located on the 3′,6′ and 3″,6″ positions play a more important role in stabilizing the doubly reduced species. The more highly fluorinated compounds $\mathbf{10F_t}$ and $\mathbf{2F_c10F_t}$ are more readily reduced than the other distyrylbenzene derivatives. At −8 °C, $\mathbf{10F_t}$ shows an irreversible reduction at −2.09 V (Figure 6b). The reduction of $\mathbf{2F_c10F_t}$ is also irreversible (−1.91 V).

By combining the electrochemical and absorption data, we can estimate absolute orbital energies. LUMO energies can be determined from the first reduction potentials.[40,41] The HOMO energy levels (Table 4) can be calculated from the LUMO and the HOMO−LUMO band gap (determined from the onset of absorption; i.e., 10% of the wavelength maxima).[8] The effect of fluorination on HOMO and LUMO energy levels is shown in Table 4.

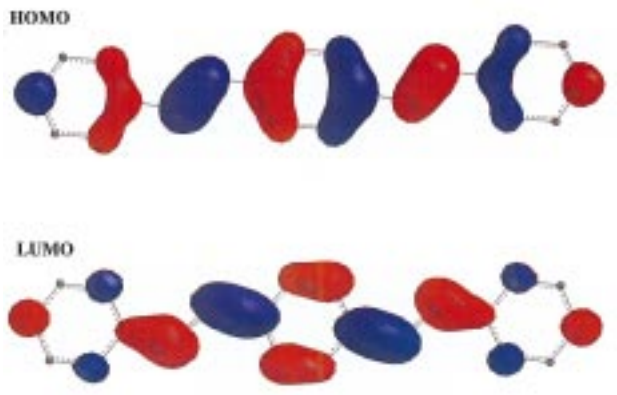

Figure 7. LUMO and HOMO of **DSB**. The surface represents a density of 0.002 electrons/au^3.

A qualitative look at the molecular orbitals of **DSB** is useful to understand the variation of the LUMO energy with fluorine regiochemistry. Fluorine substitution makes the carbon it is attached to more electronegative by inductive mechanisms,[42] decreasing the energy of the MO that the carbon contributes to.[43] Carbon atoms adjacent to the fluorinated site are affected to a lesser, but substantial, extent. Fluorine on an aromatic framework may also raise the MO energy by back-donation of π electrons. The relative contribution of these two counterbalancing effects ultimately determines the final MO energy.[44] We have not made an attempt to calculate precisely the percent contribution of different atoms to the LUMO and the resulting orbital energies for all of the fluorinated derivatives. Instead, in Figure 7, we show the HOMO and the LUMO surfaces of **DSB** determined by Hartree−Fock SCF calculations performed using Spartan 5.01. The most significant observation is that carbons 3′, 5′, 3″, and 5″ do not contribute to a major extent due to orbital symmetry.[45] As such, there is no inductive stabilization by fluorine on the carbons adjacent to 4′ and 4″. The inductive effect from fluorines on the central ring (i.e., sites 2 and 5) extends to neighboring carbons 3 and 6, which are strong contributors to both the HOMO and the LUMO. These observations account readily for the lower reduction potential of $\mathbf{2F_c}$ relative to $\mathbf{2F_t}$.

X-ray Crystallography. Weak hydrogen bonds of the C−H···F−C type are of intense current interest because of their implication in regulating the arrangement of organic molecules in crystalline solids[46] and because of their ability to stabilize the secondary structure of biomolecules such as DNA.[47] The packing of molecules containing both fluorinated and nonfluorinated aromatic rings has also received attention because these groups have complementary electrostatic distributions. Often, as a result of Coulombic forces, cofacial stacks form with alternating fluorinated/nonfluorinated aromatic rings.[48] As stated in the Introduction, the organization of organic molecules in

(40) The energy level of the normal hydrogen electrode (NHE) is −4.6 eV below the zero vacuum energy level.[41] The oxidation potential of the ferrocene reference is 0.67 V versus the NHE[34] and therefore can be estimated at −5.27 eV below the zero vacuum energy level. The energies of the LUMOs for different DSB derivatives were determined using the calibration of ferrocene against the zero vacuum energy level.

(41) Bard, A. J.; Faulkner, L. R. *Electrochemical Methods-Fundamentals and Applications*; Wiley: New York, 1984; p 634.

(42) March, J. *Advanced Organic Chemistry*, 3rd ed.; Wiley-Interscience: New York, 1985.

(43) (a) Brundle, C. R.; Robin, M. B.; Kuebler, N. A. *J. Am. Chem. Soc.* **1972**, *94*, 1466. (b) Hitchcock, A. P.; Fischer, P.; Gedanken, A.; Robin, M. B. *J. Phys. Chem.* **1987**, *91*, 531.

(44) Yim, M. B.; Wood, D. E. *J. Am. Chem. Soc.* **1976**, *98*, 2053.

(45) Heller, A. *J. Chem. Phys.* **1964**, *40*, 2839.

(46) Thalladi, V. R.; Weiss, H.-H.; Bläser, D.; Boese, R.; Nangia, A.; Desiraju, G. R. *J. Am. Chem. Soc.* **1998**, *120*, 8702 and references therein.

(47) Evans, T. A.; Seddon, K. R. *Chem. Commun.* **1997**, 2024 and references therein.

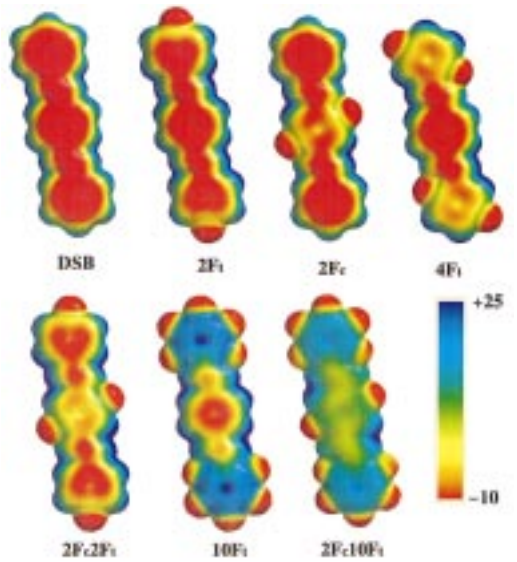

Figure 8. Electrostatic distribution plots for **DSB**, **2F$_t$**, **2F$_c$**, **2F$_c$2F$_t$**, **4F$_t$**, **10F$_t$**, and **2F$_c$10F$_t$**.

the solid impacts their performance level in a given function. With these considerations in mind we examined the solid-state arrangement of fluorinated DSBs by single-crystal X-ray diffraction techniques.

Before detailing structural data, we present the electrostatic potential maps of the compounds in this study (Figure 8). These maps, calculated using Spartan 5.0.1., will be useful when we examine the resulting packing arrangements. After performing an *ab initio* geometry optimization using the 3-21G basis set, we performed single-point energy calculations at the 6-21G level. Electrostatic potential surfaces were created for each molecule at high resolution for a density value of 0.002 electrons/au^3. Red areas correspond to regions of partial negative charge, while blue surfaces highlight regions with partial positive charge. For **DSB**, the electron density is localized at the inner core of the rings. As fluorine atoms are successively added to the distyrylbenzene framework, the electron density shifts to the periphery of the molecule (Figure 8).

X-ray structural analyses were performed on **2F$_c$**, **2F$_c$2F$_t$**, **4F$_t$**, **10F$_t$**, and **2F$_c$10F$_t$**. None of the intramolecular metrical parameters is unusual in any of these molecules, so the discussion will be focused on lattice properties. Interactions between molecules will be described as lateral contacts and end contacts as shown in Figure 9. Table 5 contains important intermolecular H···F and C···F distances and C−H···F angles.[46] Molecular axes are also defined in Figure 9.

A view of the packing of **2F$_c$** along the *b* axis (Figure 10) shows extensive $\pi-\pi$ stacking interactions, which lead to offset molecular "columns" within the crystal. A network of lateral hydrogen−fluorine contacts is observed (Figure 11) that consists primarily of interactions between the fluorine and both the olefinic H (C−H$_{olefin}$···F, 2.53 Å) and the central ring H (C−H$_{central}$···F, 2.63 Å). This network can be understood qualitatively from Figure 12. The charge distribution around the fluorine atom has considerable negative character and complements the shape and partial positive charge of the environment created by the two hydrogens.

Figure 10 might suggest that the molecular long axes (Figure 9c) across end-to-end contacts are parallel, but this is not the case. A view down the *a* axis (Figure 13) reveals that they are nearly orthogonal. In terms of electrostatics, edge-to-edge end contacts in **2F$_c$** are avoided because of the continuous partial positive character of the terminal ring edges.

A packing diagram of **2F$_c$2F$_t$** viewed along the *a* axis (Figure 14) shows once again π stacked molecular "columns". Lateral contacts are similar to those in **2F$_c$** (C−H$_{olefin}$···F, 2.56 Å). End contacts show that fluorines on the terminal rings interact with hydrogens on two neighboring molecules (H···F, 2.56 Å, 2.80 Å, see Table 5). Electrostatically, we see that the two hydrogens

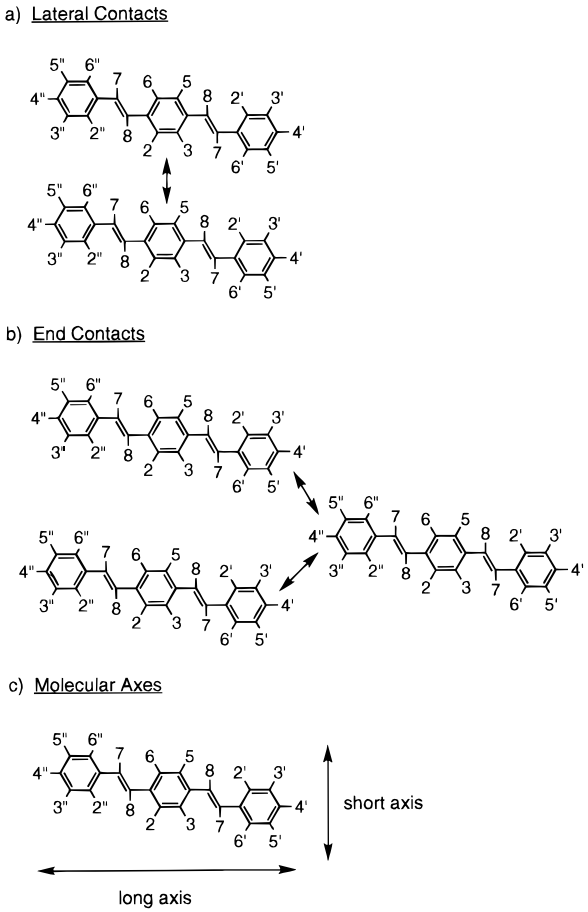

Figure 9. (a) Intermolecular lateral contacts found in the crystal lattice packing diagrams for all of the X-ray structures. (b) Intermolecular end contacts. (c) Molecular long and short axes.

Table 5. C-H···F Interactions Found in the X-ray Structures of **2F$_c$**, **2F$_c$2F$_t$**, **4F$_t$**, **10F$_t$**, and **2F$_c$10F$_t$**[a]

compound	intermolecular contacts	C−H···F	H···F (Å)[b]	C···F (Å)	C−H···F (deg)
2F$_c$	lateral	C3−H3···F5	2.63	3.48	173
	lateral	C7−H7···F5	2.53	3.57	170
2F$_c$2F$_t$	lateral	C7−H7···F5	2.56	3.47	162
	end	C3′−H3′···F4″	2.80	3.30	114
	end	C3′−H3′···F4″	2.54	3.39	149
4F$_t$	lateral	C2″−H2″···F6″	2.80	3.46	162
	lateral	C8−H8···F6″	2.54	3.72	165
	end	C4′−H4′···F3″	2.74	3.37	125
	end	C4′−H4′···F3″	2.66	3.45	141
10F$_t$	lateral	C2−H2···F2′	2.70	3.63	160
	lateral	C3−H3···F2′	2.66	3.23	119
	lateral	C7−H7···F3′	2.72	3.26	118
2F$_c$10F$_t$	lateral	C3−H3···F5	2.51	3.62	151
	lateral	C7−H7···F5	2.55	3.45	169
	lateral	F6′···H8−C8	2.76	3.50	174

[a] Intermolecular contacts and labeled molecules are shown in Figure 9. [b] Errors for intermolecular H···F distances are estimated at ±0.04 Å.

(48) Williams, J. H.; Cockcroft, J. K.; Fitch, A. N. *Angew. Chem., Int. Ed. Engl.* **1992**, *C31*, 1655.

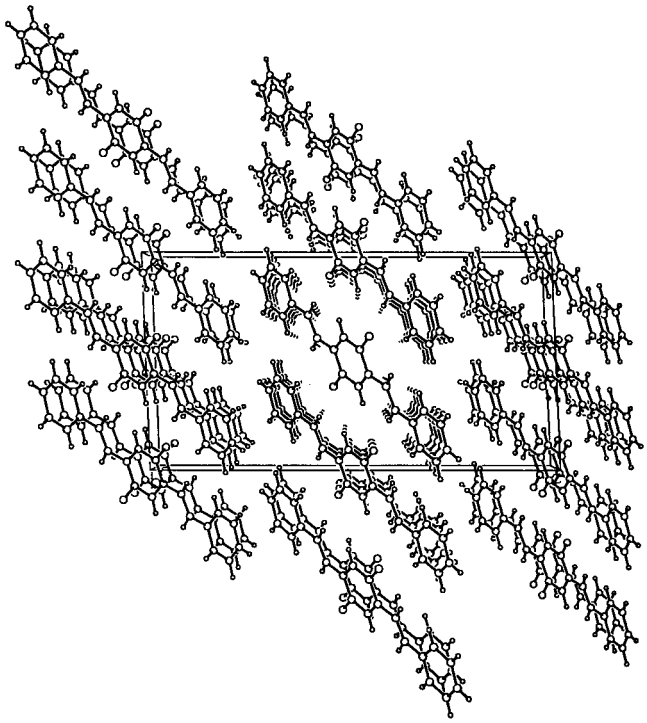

Figure 10. Molecular packing diagram of $\mathbf{2F_c}$ with a view down the *b* axis.

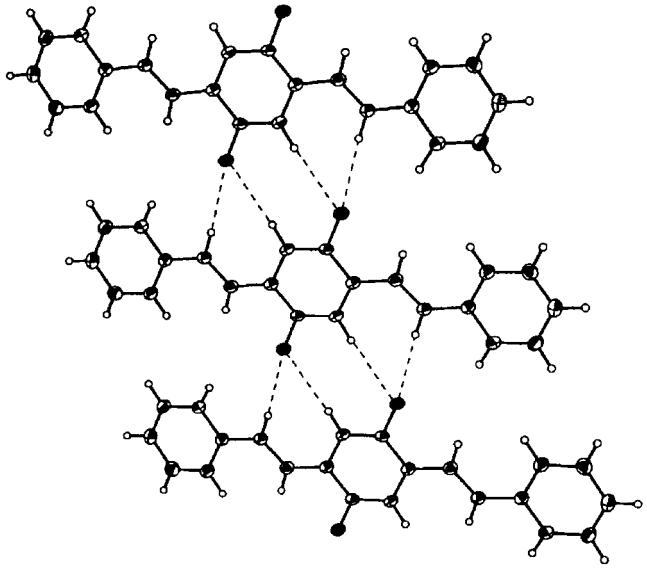

Figure 11. Molecular packing diagram of $\mathbf{2F_c}$ showing intermolecular hydrogen−fluorine contacts.

involved in the end contacts form a positive charge distribution similar in shape to that seen in the lateral contacts. In contrast to the nearly 90° angle between the molecular long axes across end contacts in $\mathbf{2F_c}$, the angle is closer to 20° in $\mathbf{2F_c2F_t}$.

The lattice parameters of $\mathbf{4F_t}$ are nearly identical to those of $\mathbf{2F_c2F_t}$ (Table 6). With the number of fluorine atoms maintained there is minimal change in the volume or density of the crystal lattice. Figure 15 illustrates the crystal packing diagram of $\mathbf{4F_t}$ down the *b* axis. Lateral interactions similar to those in the previous structures are observed with one important difference (Table 5). The H···F network involved in lateral contacts has slipped to the end ring ($C-H_{olefin}\cdots F$, 2.54 Å; $C-H_{end\ ring}\cdots F$, 2.80 Å). The H···F end contacts occur between the meta fluorine and the para hydrogens on the terminal rings of neighboring molecules. The two hydrogens form a region of partial positive

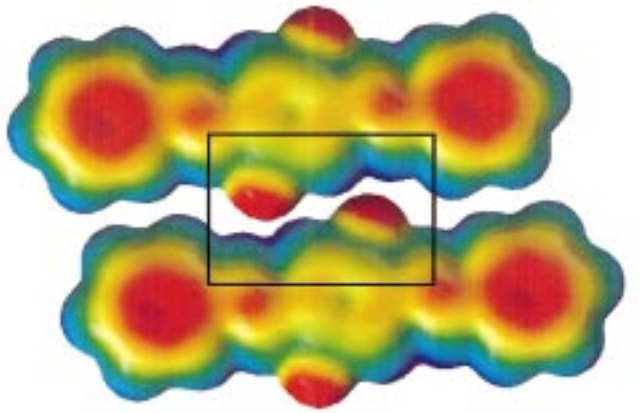

Figure 12. Electrostatic potential maps of $\mathbf{2F_c}$ showing lateral H···F contacts.

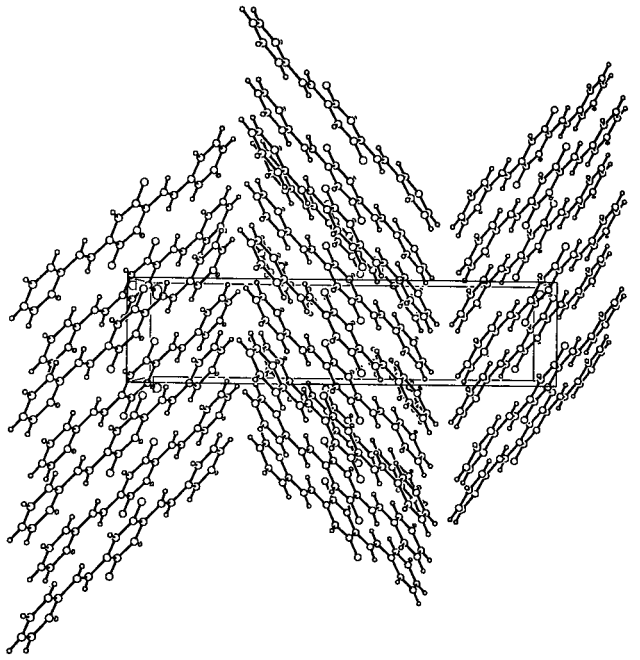

Figure 13. Molecular packing diagram of $\mathbf{2F_c}$ with a view down the *a* axis.

charge above and below the fluorine atom. Again close H···F contacts are observed (2.66 Å, 2.74 Å).

The crystal packing of both $\mathbf{2F_c10F_t}$ and $\mathbf{10F_t}$[49] shows the now familiar coplanar $\pi-\pi$ stacking (see Figure 16 for $\mathbf{2F_c10F_t}$). An additional lateral contact in $\mathbf{2F_c10F_t}$ is seen between the ortho fluorine on the terminal ring and the olefinic hydrogens (2.76 Å, Table 5). The crystal structure of $\mathbf{2F_c10F_t}$ shows that the central phenyl ring is twisted by approximately 25.1 (1)° from the plane defined by the two terminal rings. This twist minimizes steric repulsions.

In the structure of $\mathbf{2F_c}$, end contacts between molecular "columns" approach the limiting case of the benzene "T-like" structure.[50] The end result is a near orthogonal relationship between the long axes of molecules in neighboring columns. The electrostatic distribution of the terminal rings of $\mathbf{2F_c}$ might suggest that a similar arrangement could occur for the fully fluorinated terminal rings of $\mathbf{2F_c10F_t}$, which have a distribution that is similar but opposite in sign.[51] This geometry, however,

(49) Coates, G. W.; Dunn, A. R.; Henling, L. M.; Ziller, J. W.; Lobkovsky, E. B.; Grubbs, R. H. *J. Am. Chem. Soc.* **1998**, *120*, 3641.

(50) Hunter, C. A.; Sanders, J. K. M. *J. Am. Chem. Soc.* **1990**, *112*, 5525.

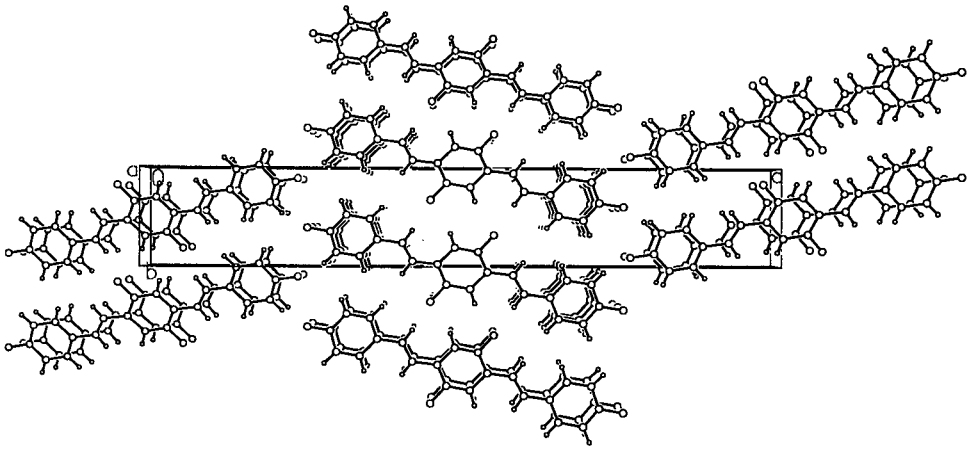

Figure 14. Molecular packing diagram of $\mathbf{2F_c2F_t}$ with a view down the *a* axis.

Table 6. Crystal and Structure Refinement Data for $\mathbf{2F_c}$, $\mathbf{2F_c2F_t}$, and $\mathbf{4F_t}$

crystal parameters	$\mathbf{2F_c}$	$\mathbf{2F_c2F_t}$	$\mathbf{4F_t}$
chemical formula	$C_{22}H_{16}F_2$	$C_{22}H_{14}F_4$	$C_{22}H_{14}F_4$
formula weight	318.35	354.33	354.33
crystal system	monoclinic	monoclinic	monoclinic
space group (no.)	*C*2/*c* (#10)	$P2_1/n$ (#14)	$P2_1/c$ (#14)
color of crystal	pale green	yellow	colorless
Z	4	2	2
a, Å	12.1979 (4)[a]	3.8377 (3)[a]	3.8757 (2)[a]
b, Å	5.5916 (2)	5.6407 (4)	5.58840 (10)
c, Å	23.1852 (4)	36.592 (3)	36.583 (2)
β, deg	92.134 (2)	92.23 (2)	91.006 (10)
volume, Å^3	1580.27 (8)	791.51 (10)	792.22 (5)
ρ_{calc}, Mg/m^3	1.338	1.487	1.485
independent reflections	1124 [R(int) = 0.0244][b]	1156 [R(int) = 0.0236][b]	1133 [R(int) = 0.0409][b]
no. of observed data	1124 ($I > 2\sigma(I)$)	1156 ($I > 2\sigma(I)$)	1133 ($I > 2\sigma(I)$)
no. of parameters varied	141	146	118
R_1[c], wR_2 %, ($I > 2\sigma(I)$)	3.93, 10.52	3.45, 8.73	3.59, 8.67
$R_1(F_o)$, $wR_2(F_o^2)$ %, all data	4.68, 11.03	3.84, 8.90	4.74, 9.1
goodness-of-fit[d]	1.060	1.086	1.048

[a] It has been noted that the integration program SAINT produces cell constant errors that are unreasonably small, since systematic error is not included. More reasonable errors might be estimated at 10× the listed values. [b] $R_{int} = \sum F_o^2 - F_o^2\,(\text{mean})|/\sum[F_o^2]$. [c] $R_1 = (\sum ||F_o| - |F_c||)/\sum |F_o|$, $wR_2 = [\sum[w(F_o^2 - F_o^2)^2]/\sum[w(F_o^2)^2]]^{1/2}$, where $w = 1/[\sigma^2(F_o^2) + (aP)^2 + bP]$ and $P = [(\text{Max};0,F_o^2) + 2F_c^2]/3$. [d] GOF $=[\sum[w(F_o^2 - F_c^2)^2]/(n - p)]^{1/2}$, where n and p denote the number of data and parameters.

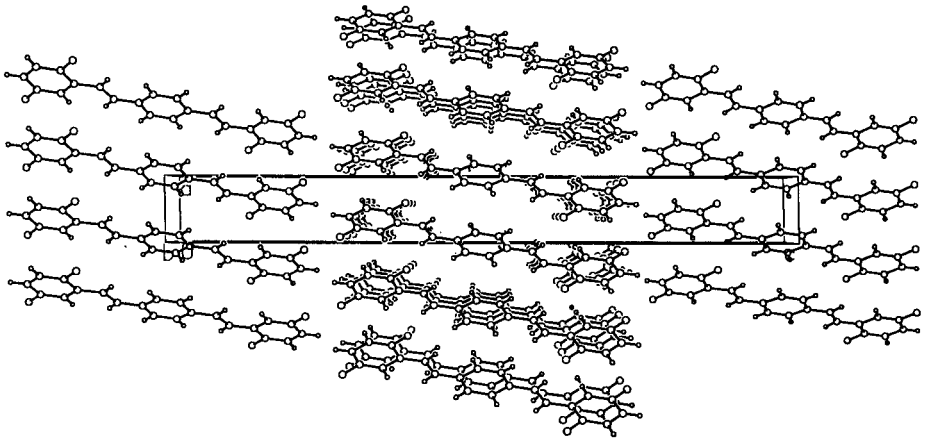

Figure 15. Molecular packing diagram of $\mathbf{4F_t}$ with a view down the *b* axis.

is not observed. For both $\mathbf{2F_c10F_t}$ and $\mathbf{10F_t}$ there is only a modest angle (15−20°) between molecules across end contacts.

Differential Scanning Calorimetry. DSC measurements complete our investigation on the effect of fluorination on bulk morphology. All compounds are crystalline and show distinct melting endotherms. The DSC thermogram of $\mathbf{2F_c}$ shown in Figure 17a shows a sharp melting endotherm at 201 °C. Similar phase transitions occur for the other derivatives with their melting points varying according to the position and number of fluorine atoms on the distyrylbenzene framework (Table 8). The thermal behavior observed for $\mathbf{10F_t}$ (Figure 17b) is different from that of the others and merits brief discussion. Three distinct

(51) Filler, R. In *Fluorine Containing Molecules Structure, Reactivity, Synthesis, and Applications*; Liebman, J. F., Greenberg, A., Dolbier, W. R., Jr., Eds.; VCH Publishers: New York, 1988; pp 19−41 and references therein.

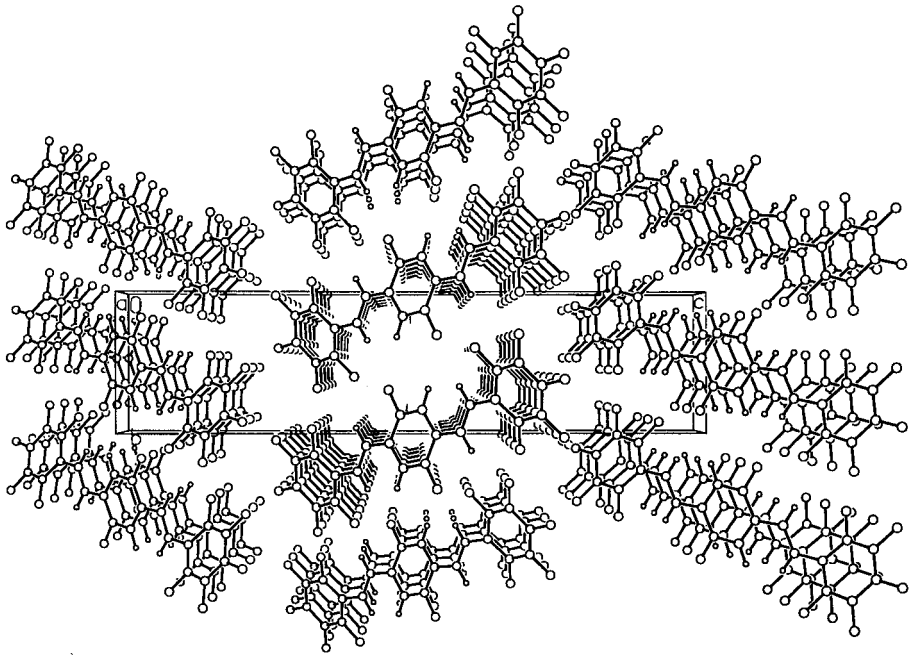

Figure 16. Molecular packing diagram of $\mathbf{2F_c10F_t}$ with a view down the *a* axis.

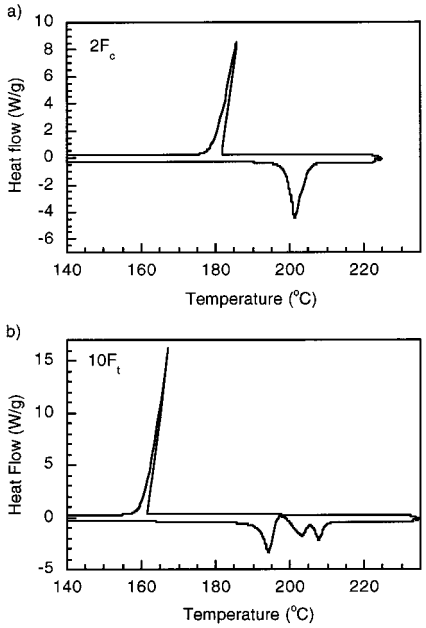

Figure 17. (a) DSC thermogram of $\mathbf{2F_c}$. Scan rate was run at 10 °C/min. (b) DSC thermogram of $\mathbf{10F_t}$. Scan rate was run at 10 °C/min.

endothermic phase transitions are observed at 194, 203, and 208 °C. The relative contribution from these depends on heating/cooling rates and sample history. The reproducibility of these transitions, together with the sample purity, suggests that there are three crystal forms or liquid crystal states closely spaced in energy.

Summary and Conclusion

We have shown that it is possible to prepare a series of fluorinated distyrylbenzene derivatives in a modular fashion. The methods used, namely, the Wittig and the Heck reactions, have proven suitable in accessing a range of conjugated organic structures.[52] As such, the success of the reactions shown in eqs 1−3 suggests new approaches for the design of fluorinated organic solids with electron affinities suitable for device applications.[7]

Table 7. Crystal and Structure Refinement Data for $\mathbf{10F_t}$ and $\mathbf{2F_c10F_t}$

crystal parameters	$\mathbf{10F_t}$	$\mathbf{2F_c10F_t}$
chemical formula	$C_{22}H_8F_{10}$	$C_{22}H_6F_{12}$
formula weight	462.28	498.27
crystal system	monoclinic	monoclinic
space group (No.)	$P2_1/c$ (#14)	$P2_1/c$ (#14)
color of crystal	colorless	colorless
Z	2	2
a, Å	4.8799 (3)[a]	4.829 (2)[a]
b, Å	6.1650 (3)	6.641 (2)
c, Å	29.533 (2)	28.019 (13)
β, deg	92.001 (2)	92.28 (3)
volume, Å^3	887.93 (9)	897.8 (6)
ρ_{calc}, Mg/m^3	1.729	1.843
independent reflections	1246 [R(int) = 0.0422][b]	1173 [R(int) = 0.0535][b]
no. of observed data	1246 ($I > 2\sigma(I)$)	1173 ($I > 2\sigma(I)$)
no. of parameters varied	145	154
R_1[c], wR_2 %, ($I > 2\sigma(I)$)	7.71, 21.34	7.98, 15.33
$R_1(F_o)$, $wR_2(F_o^2)$ %, all data	9.75, 22.26	12.78, 17.40
goodness-of-fit[d]	1.303	1.105

[a] It has been noted that the integration program SAINT produces cell constant errors that are unreasonably small, since systematic error is not included. More reasonable errors might be estimated at 10× the listed values. [b] $R_{int} = \sum|F_o^2 - F_o^2\ (\text{mean})|/\sum[F_o^2]$. [c] $R_1 = (\sum\ ||F_o| - |F_c||)/\sum\ |F_o|$, $wR_2 = [\sum[w(F_o^2 - F_o^2)^2]/\sum[w(F_o^2)^2]]^{1/2}$, where $w = 1/[\sigma^2(F_o^2) + (aP)^2 + bP]$ and $P = [(\text{Max};0,F_o^2) + 2F_o^2]/3$. [d] GOF $=[\sum[w(F_o^2 - F_c^2)^2]/(n - p)]^{1/2}$, where n and p denote the number of data and parameters.

Table 8. Melting Temperature (T_m) and Crystallization Temperature (T_c) from DSC Analysis

compound	T_m (°C)	T_c (°C)	compound	T_m (°C)	T_c (°C)
DSB	268	261	$\mathbf{4F_t}$	218	212
$\mathbf{2F_t}$	269	262	$\mathbf{10F_t}$	194, 203, 208	167
$\mathbf{2F_c}$	201	186	$\mathbf{2F_c10F_t}$	207	187
$\mathbf{2F_c2F_t}$	222	216			

The varying levels of fluorine substitution allow us to make several noteworthy observations. First, the location of the

(52) Müllen, K.; Wegner, G. *Electronic Materials: The Oligomer Approach*; WILEY−VCH: Weinheim, Germany, 1998 and references therein.

fluorine atoms within the distyrylbenzene framework impacts the ability of these atoms to facilitate reduction. This effect is exemplified by the lower reduction potential of $\mathbf{2F_c}$ relative to $\mathbf{2F_t}$ (Table 3). Concurrently, fluorine substitution does not affect the HOMO−LUMO energy gap, with all compounds absorbing and emitting at nearly identical frequencies. The molecular orbital description of **DSB**, shown in Figure 7, provides a simple rationale for these trends. The electron affinity, and thus the reduction potential, is directly related to the energy of the LUMO. Because of symmetry, different carbon atoms contribute differently to the LUMO, depending on their location. In particular, the LUMO is insensitive to any effect from carbons 3′, 5′, 3″, and 5″, where MO nodes are situated. Any inductive influence on these carbons therefore is not reflected on the energy of the LUMO. The absence of a contribution from the 3′, 5′, 3″, and 5″ carbons is also repeated in the HOMO. The similarity in symmetry of the HOMO and LUMO effectively conserves the value of the band gap, while the differences in the contributions from carbons in terminal and central environments dictate the observed trend in changes of reduction potential with respect to substitution position.

The low fluorescence quantum yield of $\mathbf{10F_t}$ stands apart from the performance of **DSB** and the other fluorinated derivatives. On the basis of the evidence collected thus far, in particular the increase of quantum yield with increasing medium viscosity and the photoisomerization results, it is likely that the excited state of $\mathbf{10F_t}$ relaxes by twisting motions around the olefinic double bonds. It is likely that, in the solid state, where molecular mobility is restricted, considerations of this type are less important.

Addition of DMA to the fluorinated DSBs results in exciplex emission. Due to a strong charge-transfer component,[53] the energy of exciplex emission is strongly dependent on the electron affinity of the acceptor molecule and the ionization potential of the donor. The energy of the exciplex emission maximum (E_{ex}) in a nonpolar solvent can be related to the donor oxidation potential (E_D^{ox}) and acceptor reduction potential (E_A^{red}) using the Weller equation:[54]

$$E_{ex} = E_D^{ox} - E_A^{red} - 0.15 \pm 0.1 \text{ eV}$$

In the case of stilbenes, a linear correlation exists between the energy of the exciplex emission and the difference between stilbene and 9,10-dicyanoanthracene redox potentials.[55] Coupling the results from our electrochemical studies to the data in Figure 5 allows a similar analysis. As shown in Figure 18, a linear relationship is observed between the energy of exciplex emission and the difference between the oxidation potential of DMA and the reduction potential of the monomer. Since the oxidation potential for DMA remains constant, the energy of the exciplex emission is related to the reduction potential of the distyrylbenzene chromophores. The variation of exciplex emission shown in Figure 5 is thus naturally explained once the redox potential of the molecules has been obtained. Further, these results indicate that the Weller equation may be a useful guideline for fine-tuning the optical properties of materials.

The overall fluorescence quantum yield was enhanced by approximately 4-fold when DMA was added to a solution of $\mathbf{10F_t}$. This increase suggests that exciplex formation is an efficient pathway, competing with other nonradiative decay pathways and that exciplex emission is also efficient. In the case of $\mathbf{2F_c10F_t}$ the overall fluorescence emission is quenched by DMA. Due to the high electron affinity of $\mathbf{2F_c10F_t}$, the formation of a nonemissive $\mathbf{2F_c10F_t}$/DMA contact radical ion pair appears to be favored.

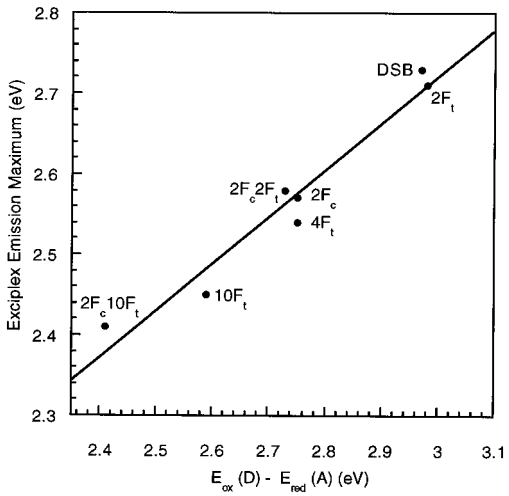

Figure 18. Comparison of the observed energy at the exciplex emission maximum (λ_{max}) and the calculated energy based on the equation E_{ox} (D) − E_{red} (A), where E_{ox} (D) is the oxidation potential of the donor and E_{red} (A) is the reduction potential of the acceptor.

A counterintuitive result from Table 3 is that, although increasing the number of fluorine atoms facilitates the addition of an electron, it does not necessarily lead to more stable radical anions! Compounds $\mathbf{10F_t}$ and $\mathbf{2F_c10F_t}$ display irreversible reductions, despite their low reduction potentials. One possibility is that, as the fluorine load increases, the radical anions eliminate fluoride more readily.[56] Optimizing the ease of reduction against durability by using fluorine substitution will likely remain a balancing act.

Two dominant packing motifs are observed in the crystallographic data presented. First, vertical stacking of aromatic rings, which is a common feature of substituted PPV oligomers,[57] is observed in all compounds. Second, the resulting vertical stacks are organized such that H···F interactions between them are optimized. A recent report has shown that, for fluoroaromatic compounds, C−H···F interactions, although weak, contribute significantly to the organization of molecules in the crystalline state.[46] These interactions may be viewed as supramolecular synthons for topological control and are important considerations for the design and engineering of amorphous and crystalline organic materials.[58] At our current stage, we can understand structures on the basis of interchromophore stacking and C−H···F interactions once the lattice arrangement has been elucidated. It is difficult, however, to predict lattice organization from molecular connectivity. Further, the DSC analysis of $\mathbf{10F_t}$ serves as a warning that polymorphism may occur.[59] Despite efforts to optimize functionality to achieve a target lattice with specific intermolecular distance and orientation, one may find that higher-energy arrangements are attained kinetically.

(53) Klessinger, M.; Michl, J. *Excited States and Photochemistry of Organic Molecules*, VCH Publishers: New York, 1995; pp 281−283.
(54) Weller, A. *Z. Phys. Chem. (Wiesbaden)* **1982**, *133*, 93.
(55) Luis, F. D.; Dykstra, R. E. *J. Photochem. Photobiol., A* **1989**, *49*, 109−119.
(56) Symons, M. C. R.; Selby, R. C.; Smith, I. G.; Bratt, S. W. *Chem. Phys. Lett.* **1977**, *48* (1), 100.
(57) Gill, R. E.; Hilberer, A.; Van Hutten, P. F.; Berentschot, G.; Werts, M. P. L.; Meetsma, A.; Wittmann, J.-C.; Hadziioannou, G. *Synth. Met.* **1997**, *84*, 637.
(58) Desiraju, G. R. *Angew. Chem., Int. Ed. Engl.* **1995**, *34*, 2311.
(59) Two polymorphs are known for 1,2,3,4-tetrafluorobenzene. Strong C−H···F interactions are observed in both instances. See ref 46 and Kottke, T.; Sunk, K.; Lagow, R. J. *Angew. Chem., Int. Ed. Engl.* **1995**, *34*, 1517.

Experimental Section

General Details. All synthetic manipulations were performed under inert atmosphere in a nitrogen-filled glovebox and using Schlenk techniques. 1,4-Diiodobenzene, 2,5-difluorobenzaldehyde, anhydrous *N*,*N*-dimethylacetamide, and *N*,*N*-dimethylaniline (DMA) were obtained from Aldrich, and styrene was obtained from Sigma. DMA was vacuum distilled from CaH and stored under nitrogen. All other reagents was used as received from Lancaster. Spectroscopic grade hexanes was vacuum distilled from CaH for exciplex studies. The quantum yield standard, 9,10-diphenylanthracene, was obtained from Aldrich and was purified by column chromatography using petroleum ether.

^{1}H NMR spectra were obtained on a Varian Unity 400 MHz spectrometer. ^{13}C NMR spectra were obtained on a Bruker AMX-400 NMR spectrometer. ^{19}F NMR spectra were obtained on a Varian Unity 500 MHz spectrometer. ^{19}F NMR chemical shifts are reported in parts per million relative to the external standard (α,α,α)-trifluorotoluene. UV−Vis absorption spectra were recorded on a Shimadzu UV-2401 PC diode array spectrophotometer and photoluminescence spectra on a Spex Fluoromax-2 spectrometer. Conditions for the time-correlated, single photon counting experiments have been reported in detail elsewhere.[60] Differential scanning calorimetry measurements were performed on a TA Instruments DSC 2920 modulated differential scanning calorimeter.

General Procedure for Heck Reaction. Reactions were carried out under phase-transfer conditions in a 14/20, 50 mL round-bottom flask equipped with a stir bar. 1,4-Diiodobenzene or 1,4-dibromo-2,5-difluorobenzene, $Pd(OAc)_2$, nBu$_4$NBr, and K_2CO_3 were stirred in 10 mL of dry *N*,*N*-dimethylacetamide at room temperature for 10 min in a nitrogen-filled glovebox. The round-bottom flask was capped with a rubber septum, wired closed, and removed from the glovebox. Styrene, 4-fluorostyrene, or pentafluorostyrene was then added to the reaction mixture via a nitrogen-purged syringe, and the mixture was stirred at 100 °C for 36 h. After cooling to room temperature, the mixture was diluted with CH_2Cl_2 and filtered through Celite. The work up of the filtrate varies depending on the compound. In some cases, product precipitated directly from the filtrate. Methanol may be used to precipitate additional product. For the more soluble compounds, the filtrate was washed three times with water, dried over $MgSO_4$ and filtered. The solvent was then removed under reduced pressure, and the remaining solid was redissolved in an appropriate solvent. The product was then purified by crystallization or by column chromatography.

1,4-Distyrylbenzene (DSB). 1,4-Distyrylbenzene was synthesized from *p*-xylylenebis(triphenylphosphonium) bromide (5.00 g, 6.34 mmol) and benzaldehyde (1.45 g, 13.7 mmol) via the Wittig route using a known literature procedure.[61] The product was obtained as a pale green crystalline solid. ^{1}H NMR (CD_2Cl_2) δ 7.55 (m, 4H), 7.54 (s, 4H), 7.37 (m, 4H), 7.27 (tt, 2H, J_{HH} = 7.33 Hz, 1.22 Hz), 7.17 (d, 2H, vinylene, J_{HH} = 16.5 Hz), 7.11 (d, 2H, vinylene, J_{HH} = 16.4 Hz); ^{13}C NMR (CD_2Cl_2) δ 136.9, 136.4, 128.3, 128.1, 127.8, 127.3, 126.5, 126.1; IR (KBr) υ_{max} 3055 (w), 3024 (w), 1447 (m), 1072 (m), 969 (s), 871 (m), 814 (s), 743 (s), 691 (s), 593 (m), 546 (s) cm^{-1}. Anal. calcd for $C_{22}H_{18}$: C, 93.58; H, 6.42. Found: C, 93.57; H, 6.47.

1,4-Bis(styryl)-2,5-difluorobenzene ($2F_c$). The general procedure described above was followed using 1,4-dibromo-2,5-difluorobenzene (1.04 g, 3.80 mmol) and styrene (1.0 g, 9.6 mmol) in the presence of $Pd(OAc)_2$ (22 mg, 0.096 mmol), nBu$_4$NBr (1.30 g, 4.03 mmol), and K_2CO_3 (1.3 g, 9.6 mmol). The filtrate was washed 3 times with water, dried over $MgSO_4$, and filtered. A pale yellow solid was crystallized from a 50:50 CH_2Cl_2/hexanes solution of the crude. Yield: 0.97 g (79%). ^{1}H NMR (CD_2Cl_2) δ 7.56 (d, 4H, J_{HH} = 8.06 Hz), 7.39 (m, 4H), 7.35 (t, 2H, J_{HF} = 8.91 Hz), 7.31 (tt, 2H, J_{HH} = 7.33 Hz, 1.22 Hz), 7.25 (d, 2H, vinylene, J_{HH} = 16.5 Hz), 7.19 (d, 2H, vinylene, J_{HH} = 16.5 Hz); ^{19}F NMR (CD_2Cl_2) δ 77.0 (t, 2F, J_{FH} = 8.93 Hz); IR (KBr) υ_{max} 3055 (w), 3022 (w), 1499 (m), 1482 (m), 1428 (s), 1263 (s), 1159 (s), 965 (s), 908 (m), 880 (s), 755 (s), 712 (m), 689 (s), 599 (m), 502 (m). Anal. calcd for $C_{22}H_{16}F_2$: C, 83.00; H, 5.07; F, 11.93. Found: C, 83.25; H, 4.97; F, 11.85.

1,4-Bis(4-fluorostyryl)benzene ($2F_t$). The general procedure described above was followed using 1,4-diiodobenzene (0.540 g, 1.64 mmol) and 4-fluorostyrene (0.50 g, 4.1 mmol) in the presence of $Pd(OAc)_2$ (9.18 mg, 0.041 mmol), nBu$_4$NBr (0.550 g, 1.72 mmol), and K_2CO_3 (0.57 g, 4.1 mmol). An off-white solid precipitated from the filtrate. Methanol was then added to the remaining filtrate to precipitate the rest of the product from solution giving an initial crude yield of 0.39 g (75%). The product was recrystallized from acetone as a pale yellow−green solid. Yield: 0.26 g (50%). ^{1}H NMR ($(CD_3)_2CO$) δ 7.71 (m, 4H), 7.65 (s, 4H), 7.33 (d, 2H, vinylene, J_{HH} = 16.2 Hz), 7.26 (d, 2H, vinylene, J_{HH} = 16.5 Hz), 7.19 (m, 4H); ^{19}F NMR (CD_2Cl_2) δ 86.5 (m, 2F); IR (KBr) υ_{max} 3041 (w), 3020 (w), 1599 (m), 1516 (s), 1506 (s), 1247 (s), 1159 (m), 1097 (m), 970 (s), 838 (s), 769 (m), 547 (s), 530 (m). Anal. calcd for $C_{22}H_{16}F_2$: C, 83.00; H, 5.07; F, 11.93. Found: C, 82.77; H, 5.15; F, 12.01.

1,4-Bis(4-fluorostyryl)-2,5-difluorobenzene ($2F_c2F_t$). The general procedure described above was followed using 1,4-dibromo-2,5-difluorobenzene (0.88 g, 3.3 mmol) and 4-fluorostyrene (1.0 g, 8.2 mmol) in the presence of $Pd(OAc)_2$ (18.4 mg, 0.082 mmol), nBu$_4$NBr (1.1 g, 3.4 mmol), and K_2CO_3 (1.1 g, 8.2 mmol). The filtrate was washed 3 times with water, dried over $MgSO_4$, and filtered. Yellow, needle-shaped crystals formed from a THF solution of the crude. Yield: 0.61 g (50%). ^{1}H NMR (CD_2Cl_2) δ 7.55 (m, 4H), 7.33 (t, 2H, J_{HF} = 8.78 Hz), 7.18 (d, 2H, vinylene, J_{HH} = 16.5 Hz), 7.0 (d, 2H, vinylene), 7.09 (m, 4H); ^{19}F NMR (CD_2Cl_2) δ 87.6 (m, 2F), 77.1 (t, 2F, J_{FH} = 8.93 Hz); IR (KBr) υ_{max} 3051 (w), 3032 (w), 1602 (s), 1512 (s), 1491 (s), 1429 (s), 1294 (m), 1244 (s), 1163 (s), 957 (s), 873 (m), 854 (s), 810 (s), 781 (m), 709 (s), 540 (m), 509 (s), 458 (m). Anal. calcd for $C_{22}H_{14}F_4$: C, 74.58; H, 3.98; F, 21.44. Found: C, 74.91; H, 4.05; F, 21.18.

1,4-Bis(2,5-difluorostyryl)benzene($4F_t$). *p*-Xylylenebis(triphenylphosphonium) bromide (2.60 g, 3.25 mmol) was suspended in 10 mL of ethanol under a positive flow of nitrogen in a 250 mL round-bottom flask. A freshly prepared solution of lithium ethoxide in ethanol (35 mL, 0.2 M) was transferred via cannula to the suspension of the bisphosphonium salt. The mixture turned yellow upon the addition of the base. After the mixture was stirred for 3 h at room temperature (RT), 2,5-difluorobenzaldehyde (1.00 g, 7.04 mmol) was added to the ylide via syringe and the reaction was stirred for an additional 24 h at RT. The reaction mixture was then diluted with 200 mL of water. A pasty yellow solid formed upon stirring overnight. The solid was filtered and redissolved in acetone. The crude product was purified via column chromatography using 2:98 toluene/hexanes. A yellow/white solid was collected. The all-trans isomer was obtained by refluxing the compound in xylenes with a trace amount of iodine. Upon cooling to room temperature a pale yellow solid precipitated from solution. The product was recrystallized twice from acetone to give **$4F_t$** as yellow needle shaped crystals. Yield: 0.12 g (10%). ^{1}H NMR (CD_2Cl_2) δ 7.58 (s, 4H), 7.34 (m, 2H), 7.28 (d, 2H, vinylene, J_{HH} = 16.7 Hz), 7.19 (d, 2H, vinylene, J_{HH} = 16.5 Hz), 7.07 (m, 2H), 6.95 (m, 2H); ^{1}H {^{19}F} NMR (CD_2Cl_2) δ 7.58 (s, 4H), 7.34 (d, 2H, J_{HH} = 2.93 Hz), 7.28 (d, 2H, vinylene, J_{HH} = 16.7 Hz), 7.19 (d, 2H, vinylene, J_{HH} = 16.5 Hz), 7.07 (d, 2H, J_{HH} = 8.79 Hz), 6.95 (dd, 2H, J_{HH} = 9.16 Hz, 2.93 Hz); ^{19}F NMR (CD_2Cl_2) δ 81.7 (m, 2F), 76.9 (m, 2F); IR (KBr) υ_{max} 3077 (w), 3062 (w), 1489 (s), 1270 (m), 1243 (m), 1191 (m), 1178 (m), 1140 (m), 1088 (m), 957 (s), 856 (s), 796 (s), 729 (s), 513 (s). Anal. calcd for $C_{22}H_{14}F_4$: C, 74.58; H, 3.98; F, 21.44. Found: C, 74.23; H, 4.16; F, 21.25.

1,4-Bis(2,3,4,5,6-pentafluorostyryl)benzene ($10F_t$). The general procedure described above was followed using 1,4-diiodobenzene (0.680 g, 2.06 mmol) and 2,3,4,5,6-pentafluorostyrene (1.0 g, 5.2 mmol) in the presence of $Pd(OAc)_2$ (11.7 mg, 0.052 mmol), nBu$_4$NBr (0.70 g, 2.2 mmol), and K_2CO_3 (0.72 g, 5.2 mmol). The filtrate was washed 3 times with water and one time with 0.1 M HCl (aq). The solution was then dried over $MgSO_4$ and filtered. The crude product was reduced in volume and purified by column chromatography using hexanes. **$10F_t$** was collected as a pale green solid. Yield: 0.60 g (63%). Spectral data and physical properties matched those previously reported.[62] ^{1}H NMR (CD_2Cl_2) δ 7.59 (s, 4H), 7.46 (d, 2H, vinylene, J_{HH} = 16. 8), 7.06 (d,

(60) Khan, M. I.; Renak, M. L.; Bazan, G. C.; Popovic, Z. *J. Am. Chem. Soc.* **1997**, *119*, 5344.

(61) Campbell, T. W.; McDonald, R. N. *J. Org. Chem.* **1959**, *24*, 1246.

2H, vinylene, J_{HH} = 16.8 Hz); ^{19}F NMR (CD_2Cl_2) δ 58.2 (m, 4F), 44.15 (t, 2F, J_{FF} = 20.9 Hz), 37.5 (m, 4F); IR (KBr) υ_{max} 3072 (w), 3031 (w), 1524 (s), 1494 (s), 1426 (m), 1422 (m), 1337 (m), 1136 (m), 1001 (s), 964 (s), 808 (m), 652 (m), 518 (m). Anal. calcd for $C_{22}H_8F_{10}$: C, 57.16; H, 1.74; F, 41.10. Found: C, 57.04; H, 1.61; F, 41.36.

1,4-Bis(2,3,4,5,6-pentafluorostyryl)-2,5-difluorobenzene ($2F_c10F_t$). The general procedure described above was followed using 1,4-dibromo-2,5-difluorobenzene (0.280 g, 1.03 mmol) and 2,3,4,5,6-pentafluorostyrene (0.50 g, 2.6 mmol) in the presence of $Pd(OAc)_2$ (5.8 mg, 0.026 mmol), nBu$_4$NBr (0.350 g, 1.08 mmol), and K_2CO_3 (0.36 g, 2.6 mmol). The orange/brown filtrate was washed 3 times with water and once with 0.1 M HCl (aq). The solution was dried over $MgSO_4$ and filtered. The crude product was reduced in volume and purified by column chromatography using hexanes. A pale yellow−green solid was collected and recrystallized from acetone. Yield: 0.13 g (25%). ^{1}H NMR (CD_2Cl_2) δ 7.53 (d, 2H, vinylene, J_{HH} = 17 Hz), 7.39 (t, 2H, J_{HF} = 8.66 Hz), 7.11 (d, 2H, vinylene, J_{HH} = 16.8 Hz); ^{19}F NMR (CD_2Cl_2) δ 78.6 (t, 2F, J_{FH} = 8.93 Hz), 58.7 (m, 4F), 45.6 (t, 2F, J_{FF} = 20.9 Hz), 37.9 (m, 4F); IR (KBr) υ_{max} 1522 (s), 1495 (s), 1428 (s), 1353 (m), 1258 (m), 1164 (m), 1135 (m), 1004 (s), 973 (s), 962 (s), 903 (m), 881 (m), 700 (m), 653 (m), 577 (w). Anal. calcd for $C_{22}H_6F_{12}$: C, 53.04; H, 1.21; F, 45.75. Found: C, 53.17; H, 1.36; F, 45.18.

Quantum Yield Determinations. Solutions for fluorescence measurements were prepared from saturated solutions of the compounds in degassed cyclohexane. Approximately 1 mg of compound was stirred in 5 mL of cyclohexane for 5 min at RT. The mixture was filtered through a 0.45 μm syringe filter, and the resulting solution was diluted so that the absorbance maximum was approximately 0.1. All manipulations were performed inside a glovebox, and the solutions were introduced into a 1 cm quartz cuvette equipped with a Teflon needle valve to avoid contact with air. Fluorescence was measured at right angles using an excitation wavelength of 350 nm. The quantum yield was calculated from the relation:[63]

$$\phi_u = \phi_s[(A(\lambda)_s F_u n_u^2)/(A(\lambda)_u F_s n_s^2)]$$

where the subscripts s and u indicate the standard and unknown sample, $A(\lambda)$ corresponds to the absorbance of the solution at the exciting wavelength λ, F is the integrated luminescence spectrum, and n is the index of refraction for the solvent carrying the unknown and the standard at the sodium D line (assumed equal for all measurements). The standard fluorophore for solution measurements was 9,10-diphenylanthracene[27] with Φ_{PL} = 0.90.

Exciplex Studies. Solutions for absorbance and fluorescence measurements were prepared in a nitrogen-filled glovebox. The solutions were introduced into a 1 × 1 cm quartz cuvette equipped with a Teflon needle valve to avoid contact with air. Fluorescence was measured at room temperature at right angles using an excitation wavelength of 350 nm.

A 1×10^{-4} M solution of **DSB** in dry hexanes was prepared in a 50 mL volumetric flask. A 0.3 mL aliquot of the resulting stock solution was placed into a 10 mL volumetric flask and diluted with hexanes, giving a 3×10^{-6} M solution of **DSB**. To prepare a combined solution of **DSB** (3×10^{-6} M) and DMA (0.1 M), we added 0.3 mL of the 1×10^{-4} M **DSB** stock solution and 0.13 mL of neat DMA to a 10 mL volumetric flask and diluted the mixture with hexanes. Measurements for all fluorinated DSB derivatives were prepared in the manner described above.

Electrochemical Measurements. Cyclic voltammograms of all of the compounds except **DSB** were measured in a nitrogen-filled glovebox using an EG&G PAR 173 potentiostat equipped with a model 276 insert. A standard 3 electrode configuration was used with a Pt disk (0.25 mm in diameter) working electrode, a Pt wire counter electrode, and a bare silver wire reference electrode. Cyclic voltammograms of **DSB** were performed on the benchtop under vacuum using a EG&G PAR 273 potentiostat. A three electrode cell was used with a Pt disk working electrode (0.7 mm in diameter), a Pt wire counter electrode, and a bare silver wire reference electrode.

The THF solvent was dried over sodium/benzophenone and vacuum transferred immediately before each use. Cyclic voltammetry measurements were performed using 0.001 M analyte in 0.2 M (nBu$_4$N)(PF_6)/THF. All measurements were done at room temperature and at a scan rate of 200 mV/s unless otherwise noted. Potentials were calibrated against the formal potential of the ferrocene/ferrocenium (Fc/Fc^+) couple using decamethylferrocene ($Me_{10}Fc$) as the internal standard (Fc vs $Me_{10}Fc$ is 0.449 V in THF).[37]

X-ray Structural Determination of $2F_c$, $2F_c2F_t$, $4F_t$, $10F_t$, and $2F_c10F_t$. The X-ray intensity data were collected on a standard Siemens SMART CCD area detector system equipped with a normal focus molybdenum-target X-ray tube operated at 2.0 kW (50 kV, 40 mA). A total of 1321 frames of data (1.3 hemispheres) were collected using a narrow frame method with scan widths of 0.3° in w and exposure times of either 30 s/frame ($2F_c$, $2F_c2F_t$, and $4F_t$) or 60 s/frame ($10F_t$ and $2F_c10F_t$) using a detector-to-crystal distance of 5.09 cm (maximum 2θ angle of 56.6°). The total data collection time was approximately either 12 or 25 h, respectively, for 30 or 60 s frames. Frames were integrated to 0.90 Å with the Siemens SAINT program. Laue symmetry revealed monoclinic crystal systems for all the data sets, and the final unit cell parameters (at −80 °C) were determined from the least-squares refinement of three-dimensional centroids of 1000 reflections.[64] Data were corrected for absorption with the SADABS[65] program.

Space group assignments are provided in Tables 6 and 7. The structures were solved by using direct methods and refined employing full-matrix least-squares on F^2 (Siemens, SHELXTL,[66] version 5.04). For each of the crystals, there is half of the molecule in the asymmetric unit. All of the non-H atoms were refined anisotropically for all the data sets, and the hydrogen atoms were located and their positions and isotropic thermal parameters refined for $2F_c$ and $2F_c2F_t$. The hydrogen atoms were included in idealized positions for $4F_t$, $10F_t$, and $2F_c10F_t$. The final residuals are provided in Tables 6 and 7. Further details of the data collection, solution, and refinement can be found in the Supporting Information.

Acknowledgment. Financial support from the NSF (DMR 9500627) and the Office of Naval Research (N00014-1-0643) is gratefully acknowledged. Optical measurements were done using the NSF Center for Photoinduced Charge Transfer facilities. The authors thank Dr. Steve Atherton for the single photon counting experiments, Dr. William Geiger at the University of Vermont for use of electrochemical equipment and insightful discussions, and Dr. Mike Shaw for doing cyclic voltammetry measurements of $2F_c$ and $10F_t$ and for useful advice on cyclic voltammetry.

Supporting Information Available: Complete experimental details the X-ray crystallographic determination of $2F_c$, $2F_c2F_t$, $4F_t$, $10F_t$, and $2F_c10F_t$. This material is available free of charge via the Internet at http://pubs.acs.org.

JA984440Q

(62) See ref 49 and Filler, R.; Gadomski, J. E. *J. Fluorine Chem.* **1990**, *47*, 175.

(63) Eaton, D. F. *Pure Appl. Chem.* **1988**, *60* (7), 1107.

(64) It has been noted that the integration program SAINT produces cell constant errors that are unreasonably small, since systematic error is not included. More reasonable errors might be estimated at 10× the listed value.

(65) The SADABS program is based on the method of Blessing; see Blessing, R. H. *Acta Crystallogr., Sect A* **1995**, *51*, 33.

(66) *SHELXTL: Structure Analysis Program, version 5.04*; Siemens Industrial Automation Inc.: Madison, WI, 1995.